

# THE MENGER CURVE AND SPHERICAL CR UNIFORMIZATION OF A CLOSED HYPERBOLIC 3-ORBIFOLD

JIMING MA AND BAOHUA XIE

ABSTRACT. Let  $G_{6,3}$  be a hyperbolic polygon-group with boundary the Menger curve. Granier [11] constructed a discrete, convex cocompact and faithful representation  $\rho$  of  $G_{6,3}$  into  $\mathbf{PU}(2,1)$ . We show the 3-orbifold at infinity of  $\rho(G_{6,3})$  is a closed hyperbolic 3-orbifold, with underlying space the 3-sphere and singular locus the  $\mathbb{Z}_3$ -coned chain-link  $C(6, -2)$ . This answers the second part of Kapovich's Conjecture 10.6 in [15], and it also provides the second explicit example of a closed hyperbolic 3-orbifold that admits a uniformizable spherical CR-structure after Schwartz's first example in [26].

## 1. INTRODUCTION

Complex hyperbolic geometry is a cousin of real hyperbolic geometry, but we currently know very little about it. Let  $\mathbf{H}_{\mathbb{C}}^2$  be the complex hyperbolic plane. The holomorphic isometry group of  $\mathbf{H}_{\mathbb{C}}^2$  is  $\mathbf{PU}(2,1)$ . A *spherical CR-structure* on a smooth 3-manifold  $M$  is a maximal collection of distinguished charts modeled on the boundary  $\partial\mathbf{H}_{\mathbb{C}}^2$  of  $\mathbf{H}_{\mathbb{C}}^2$ , where coordinate changes are restrictions of transformations from  $\mathbf{PU}(2,1)$ . In other words, a spherical CR-structure is a  $(G, X)$ -structure with  $G = \mathbf{PU}(2,1)$  and  $X = \mathbb{S}^3$ . In contrast to the results on other geometric structures carried on 3-manifolds, there are relatively few examples known of spherical CR-structures. A spherical CR-structure on a 3-orbifold  $M$  is *uniformizable* if it is obtained as  $M = \Gamma \backslash \Omega_{\Gamma}$ , where  $\Omega_{\Gamma} \subset \partial\mathbf{H}_{\mathbb{C}}^2$  is the set of discontinuity of a discrete subgroup  $\Gamma$  acting on  $\partial\mathbf{H}_{\mathbb{C}}^2 = \mathbb{S}^3$ . The *limit set*  $\Lambda_{\Gamma}$  of  $\Gamma$  is by definition  $\mathbb{S}^3 - \Omega_{\Gamma}$ .

Goldman and Parker in [10] initiated the study of the deformations of the ideal triangle group in  $\mathbf{PU}(2,1)$ . They gave an interval contained in the parameter space of complex hyperbolic ideal triangle groups, for points in this interval the corresponding representations are discrete and faithful. They conjectured that a complex hyperbolic ideal triangle group  $\Gamma = \langle I_1, I_2, I_3 \rangle$  is discrete and faithful if and only if  $I_1 I_2 I_3$  is not elliptic. Schwartz proved the Goldman-Parker conjecture in [23, 27]. Furthermore, Schwartz analyzed the complex hyperbolic ideal triangle group  $\Gamma$  when  $I_1 I_2 I_3$  is parabolic and showed the 3-manifold at infinity of the quotient space  $\mathbf{H}_{\mathbb{C}}^2/\Gamma$  is commensurable with the Whitehead link complement in the 3-sphere. In other words, the Whitehead link complement admits uniformizable spherical CR-structure. Schwartz has conjectured the necessary and sufficient condition for a general complex hyperbolic  $(p, q, r)$  triangle group

---

*Date:* June 5, 2024.

*2010 Mathematics Subject Classification.* 20H10, 57M50, 22E40, 51M10.

*Key words and phrases.* Complex hyperbolic geometry, Spherical CR uniformization, Hyperbolic groups, Menger curve, Hyperbolic 3-orbifolds.

Ma was supported by NSFC (No.12171092). Xie was supported by NSFC (No.11871202, No.12271148).

$\Delta_{p,q,r} = \langle I_1, I_2, I_3 \rangle < \mathbf{PU}(2, 1)$  to be a discrete and faithful representation of an abstract triangle group  $T(p, q, r)$  [25]. Schwartz's conjecture has been proved in a few cases [4, 6, 14, 21, 22]. These complex hyperbolic triangle groups give more interesting examples that some cusped hyperbolic 3-manifolds admit uniformizable spherical CR-structures [1, 4, 6, 14, 16, 22, 24].

These complex hyperbolic triangle groups above are abstractly commensurable to a surface group or a free group. So these abstract groups are Gromov hyperbolic, with the boundary a circle or a Cantor set. For more details on hyperbolic groups and their boundaries, the reader may refer to [12]. But there are some more complicated groups that can act on  $\mathbf{H}_{\mathbb{C}}^2$  geometrically. One example is in [26], where Schwartz considered an unfaithful representation of a triangle group into  $\mathbf{PU}(2, 1)$ , the image group is called  $\Delta_{4,4,4;7}$ , which is an arithmetic, geometrically finite, discrete subgroup of  $\mathbf{PU}(2, 1)$ . Schwartz determined the 3-manifold at infinity of  $\Delta_{4,4,4;7}$  via a sophisticated method. It is conjectured that the limit set of Schwartz's group  $\Delta_{4,4,4;7}$  is a Menger curve [26].

Let

$$G_{6,3} = \langle a_0, \dots, a_5 \mid a_i^3 = id, a_i a_{i+1} = a_{i+1} a_i, i \in \mathbb{Z}/6\mathbb{Z} \rangle$$

be a hyperbolic group with boundary the Menger curve [2]. Recall that the *Menger curve*  $\mathcal{K}$  is a one-dimensional locally connected metrizable continuum without locally separating points, which contain the topological image of any curve. The *standard Menger curve in  $\mathbb{R}^3$*  can be obtained as follows: first we subdivide the standard cube  $C_0 = [0, 1]^3$  into  $3^3$  congruent subcubes; let  $C_1$  be the union of these subcubes that intersect the one-skeleton of  $C_0$ ; then we repeat this process on each subcube again and again to define  $C_n$ ; the standard Menger curve in  $\mathbb{R}^3$  is defined to be the intersection

$$\mathcal{M} = \bigcap_{n=0}^{\infty} C_n.$$

Granier [11] constructed a discrete, convex-cocompact and faithful representation  $\rho$  of  $G_{6,3}$  into  $\mathbf{PU}(2, 1)$ , so the limit set  $\Lambda$  of  $\rho(G_{6,3})$  is homeomorphic to the boundary of  $G_{6,3}$ , that is,  $\Lambda = \mathcal{K}$  topologically. See Section 3 for more details on Granier's representation.

Kapovich made the following conjecture on Granier's representation, see Conjecture 10.6 of [15]:

**Conjecture 1.1.** *The Menger curve limit set above is "unknotted" in  $\mathbb{S}^3$ , i.e., the limit set  $\Lambda$  of  $\rho(G_{6,3})$  is ambient-isotopic to the standard Menger curve  $\mathcal{M} \subset \mathbb{R}^3 \subset \mathbb{S}^3$ . Furthermore, the quotient 3-dimensional manifold  $\Omega/\rho(G_{6,3})$  is hyperbolic, where  $\Omega$  is the set of discontinuity of  $\rho(G_{6,3})$ .*

In this paper, we study the topology and geometry of the 3-orbifold  $\Omega/\rho(G_{6,3})$  at infinity of  $\rho(G_{6,3})$ . We answer the second part of Conjecture 1.1:

**Theorem 1.2.** *The 3-orbifold  $\Omega/\rho(G_{6,3})$  at infinity of  $\rho(G_{6,3})$  is a closed hyperbolic 3-orbifold  $\mathcal{O}$ , with underlying space the 3-sphere and singularity locus the  $\mathbb{Z}_3$ -coned chain-link  $C(6, -2)$ .*

To the authors' knowledge, the 3-orbifold  $\mathcal{O}$  in Theorem 1.2 is the second explicit example of a closed hyperbolic 3-orbifold that admits a uniformizable spherical CR-structure after the first example by Schwartz [26] nearly twenty years ago.

We prove Theorem 1.2 by studying the quotient of the ideal boundary of the Dirichlet domain under the action of the group  $\rho(G_{6,3})$ . Granier described a Dirichlet domain  $D$  of  $\rho(G_{6,3})$  centered at the fixed point of an elliptic element of order

6 in  $\rho(G_{6,3})$  in her thesis [11]. We will continue to study the topology of  $\partial_\infty D \cap \Omega$  in  $\mathbb{S}^3$ . We show that

**Theorem 1.3.**  *$\partial_\infty D \cap \Omega$  is a solid torus in the 3-sphere  $\partial\mathbf{H}_\mathbb{C}^2$ .*

From Figure 8 in Section 5, it seems that  $\partial_\infty D \cap \Omega$  is an unknotted solid torus in the 3-sphere  $\partial\mathbf{H}_\mathbb{C}^2$ . That is, the complement of  $\partial_\infty D \cap \Omega$  in  $\partial\mathbf{H}_\mathbb{C}^2$  is also a solid torus (we do not prove this rigorously), which seems to be strong evidence of the first part of Conjecture 1.1.

**Outline of the paper:** In Section 2, we give a well-known background material on complex hyperbolic geometry. Section 3 contains the matrix representation of the group and the Dirichlet domain constructed by Granier, and we will study carefully the combinatorial structure of the ideal boundary of the Dirichlet domain  $D$  in Sections 4 and 5. In particular, we will prove Theorem 1.3 in Section 5. We will prove Theorem 1.2 in Section 6 based on results in Sections 4 and 5.

**Acknowledgements.** We would like to thank the anonymous referees for their helpful comments and constructive suggestions that improved the manuscript. Moreover, one of the referees proposed an easy way to show the 3-orbifold in Theorem 1.2 is hyperbolic. B. Xie is grateful to the LMNS (Laboratory of Mathematics for Nonlinear Science) of Fudan University for its hospitality during his visit.

## 2. BACKGROUND

In this section, we introduce some background about complex hyperbolic geometry. Almost all facts stated here can be found in the book of Goldman [9] and in [7].

Let  $\mathbb{C}^{2,1}$  be the 3-dimensional complex vector space consisting of 3-tuples

$$Z = \begin{pmatrix} z_1 \\ z_2 \\ z_3 \end{pmatrix} \in \mathbb{C}^3$$

endowed with a Hermitian form  $\langle \cdot, \cdot \rangle$ , which has signature  $(2, 1)$ .

A vector  $Z$  is said to be negative (respectively null, positive) if and only if the Hermitian form  $\langle Z, Z \rangle$  is negative (respectively null, positive). Let  $\mathbb{P} : \mathbb{C}^{2,1} \setminus \{0\} \rightarrow \mathbb{C}\mathbb{P}^2$  be the standard projection map. *Complex hyperbolic plane*  $\mathbf{H}_\mathbb{C}^2$  is defined to be the subset of  $\mathbb{P}(\mathbb{C}^{2,1} \setminus \{0\})$  consisting of negative lines in  $\mathbb{C}^{2,1}$ . The boundary of  $\mathbf{H}_\mathbb{C}^2$  is the subset  $\partial\mathbf{H}_\mathbb{C}^2$  of  $\mathbb{P}(\mathbb{C}^{2,1} \setminus \{0\})$  consisting of null lines in  $\mathbb{C}^{2,1}$ .

In this paper, we will use two different models of complex hyperbolic plane. There are two different Hermitian matrices  $J$  which give different Hermitian forms on  $\mathbb{C}^{2,1}$ . Let  $Z, W$  be the column vectors  $(z_1, z_2, z_3)^t$  and  $(w_1, w_2, w_3)^t$  respectively. The first Hermitian form is defined to be

$$\langle Z, W \rangle = -z_1 \overline{w_1} + z_2 \overline{w_2} + z_3 \overline{w_3}.$$

It is given by the Hermitian matrix  $J_1$ :

$$J_1 = \begin{bmatrix} -1 & 0 & 0 \\ 0 & 1 & 0 \\ 0 & 0 & 1 \end{bmatrix}.$$

Note that this Hermitian form agrees with the one given in [11].

The second Hermitian form is defined to be

$$\langle Z, W \rangle = z_1 \bar{w}_3 + z_2 \bar{w}_2 + z_3 \bar{w}_1.$$

It is given by the Hermitian matrix  $J_2$ :

$$J_2 = \begin{bmatrix} 0 & 0 & 1 \\ 0 & 1 & 0 \\ 1 & 0 & 0 \end{bmatrix}.$$

We define the first model of complex hyperbolic plane by taking  $z_1 = 1$  in column vector  $Z = (z_1, z_2, z_3)^t \in \mathbb{C}^{2,1}$  for the first Hermitian form. We then have

$$\mathbf{H}_{\mathbb{C}}^2 = \left\{ \begin{pmatrix} 1 \\ z_1 \\ z_2 \end{pmatrix} \in \mathbb{C}\mathbb{P}^2 \mid |z_1|^2 + |z_2|^2 < 1 \right\}.$$

This forms the unit ball model of complex hyperbolic plane. The boundary  $\partial\mathbf{H}_{\mathbb{C}}^2$  is the sphere  $\mathbb{S}^3$  given by

$$|z_1|^2 + |z_2|^2 = 1.$$

Almost all calculations in Sections 4 and 5 will be done in the ball model. For the convenience to drawing pictures, we also consider the Siegel model. We obtain the Siegel model of complex hyperbolic plane by taking  $z_3 = 1$  in column vector  $Z = (z_1, z_2, z_3)^t \in \mathbb{C}^{2,1}$  for the second Hermitian form. That is,

$$\mathbf{H}_{\mathbb{C}}^2 = \left\{ \begin{pmatrix} z_1 \\ z_2 \\ 1 \end{pmatrix} \in \mathbb{C}\mathbb{P}^2 \mid 2\operatorname{Re}(z_1) + |z_2|^2 < 0 \right\}.$$

Its boundary  $\partial\mathbf{H}_{\mathbb{C}}^2$  is

$$\partial\mathbf{H}_{\mathbb{C}}^2 = \{(-(|z|^2 + is)/2, z, 1)^t \mid (z, s) \in \mathbb{C} \times \mathbb{R}\} \cup \{\infty = (1, 0, 0)^t\}.$$

It is also the one point compactification of the 3-dimensional Heisenberg group  $\mathbb{C} \times \mathbb{R}$ , with group law

$$[z, t] \cdot [w, s] = [z + w, t + s + 2\operatorname{Im}(z\bar{w})].$$

To move from the ball model to the Siegel model we introduce the Cayley transformation

$$C = \begin{bmatrix} \frac{1}{\sqrt{2}} & 0 & \frac{1}{\sqrt{2}} \\ 0 & 1 & 0 \\ -\frac{1}{\sqrt{2}} & 0 & \frac{1}{\sqrt{2}} \end{bmatrix}.$$

The group of linear isometries preserving the Hermitian form  $J$  is a non-compact group isomorphic to  $\mathbf{U}(2, 1)$  (with respect to  $J$ ). We denote  $\mathbf{PU}(2, 1)$  by the group of holomorphic isometries of  $\mathbf{H}_{\mathbb{C}}^2$ , which is the projectivization of the unitary group  $\mathbf{U}(2, 1)$ . We will often consider matrices in the group  $\mathbf{SU}(2, 1)$  instead of elements of  $\mathbf{PU}(2, 1)$ . Every element of  $\mathbf{PU}(2, 1)$  admits exactly three lifts to the group  $\mathbf{SU}(2, 1)$  of unitary matrices for  $J$  of determinant one.

Up to scaling,  $\mathbf{H}_{\mathbb{C}}^2$  carries a unique  $\mathbf{U}(2, 1)$ -invariant Riemannian metric with curvature between  $-1$  and  $-1/4$ . The metric information we will use is the following distance formula:

$$(2.1) \quad \cosh\left(\frac{d(u, v)}{2}\right) = \frac{|\langle \mathbf{u}, \mathbf{v} \rangle|}{\sqrt{\langle \mathbf{u}, \mathbf{u} \rangle \langle \mathbf{v}, \mathbf{v} \rangle}},$$

where  $\mathbf{u}, \mathbf{v}$  denote lifts of  $u, v$  to  $\mathbb{C}^3$ .

If  $u, v \in \mathbb{C}^3$ , we define the *Hermitian cross product* of  $u$  and  $v$ , denoted by  $u \boxtimes v$ , as the Euclidean cross product of the vectors  $u^* J$  and  $v^* J$ , where  $J$  is the matrix defining the Hermitian form,  $u^*$  and  $v^*$  are the conjugate transpose vectors of  $u$  and  $v$ . If  $u$  and  $v$  are collinear, then  $u \boxtimes v = 0$ . If not, then  $u \boxtimes v$  spans their Hermitian orthogonal complement and  $\langle u \boxtimes v, u \rangle = 0, \langle u \boxtimes v, v \rangle = 0$ .

**2.1. Totally geodesic subspace.** Given a positive vector  $v \in \mathbb{C}^{2,1}$ , its orthogonal complement  $v^\perp = \{u \in \mathbb{C}^3 : \langle v, u \rangle = 0\}$  is a two dimensional subspace on which the Hermitian form restricts to a form with signature  $(1, 1)$ . The set of negative lines in  $v^\perp$  is then a copy of  $\mathbf{H}_\mathbb{C}^1$ , naturally isometric to the Poincaré disk.

**Definition 2.1.** The submanifold of  $\mathbf{H}_\mathbb{C}^2$  given by  $v^\perp$  is called a *complex geodesic*. The vector  $v$  is called a *polar* to the complex geodesic  $v^\perp$ .

Given a vector  $v$  with  $\langle v, v \rangle = 1$ , we consider the isometry of  $\mathbb{C}^3$  given by

$$R_{v,\zeta}(x) = x + (\zeta - 1)\langle x, v \rangle v$$

where  $\zeta$  is a complex number of absolute value one. It is easy to see that  $R_{v,\zeta}(x)$  preserves the Hermitian inner product, fixes the vectors in  $v^\perp$ , and rotates the normal direction by an angle  $\theta$ , where  $\zeta = e^{i\theta}$ .

**Definition 2.2.** The isometry  $R_{v,\zeta}$  is called a *complex reflection* with mirror  $v^\perp$ .

Another type of totally geodesic subspace is given in the standard ball model as the set of points with real coordinates, which is the fixed point set of the isometry  $(x_1, x_2) \rightarrow (\bar{x}_1, \bar{x}_2)$ . It is simply a copy of the real hyperbolic plane  $\mathbf{H}_\mathbb{R}^2$ . This submanifold of  $\mathbf{H}_\mathbb{C}^2$  is often called a *Langrangian plane*.

The boundary at infinity of a complex geodesic is called  $\mathbb{C}$ -circle, and the boundary at infinity of a copy of  $\mathbf{H}_\mathbb{R}^2$  is called an  $\mathbb{R}$ -circle. The group  $\mathbf{PU}(2, 1)$  acts transitively on each kind of subspaces.

**2.2. Bisectors and their intersections.** Note that there are no totally geodesic real hypersurfaces in complex hyperbolic space. The Dirichlet polyhedra are bounded by bisectors, which are hypersurfaces equidistant from two given points. Their geometric structure and complicated intersection patterns have been analyzed in great detail in [9]. We will review some of the results which will be needed in the paper.

**Definition 2.3.** The *bisector* between two distinct points  $p_0$  and  $p_1$  in  $\mathbf{H}_\mathbb{C}^2$  is the set of points that are equidistant from  $p_0$  and  $p_1$ :

$$(2.2) \quad \mathcal{B}(p_0, p_1) = \{u \in \mathbf{H}_\mathbb{C}^2 : d(u, p_0) = d(u, p_1)\}.$$

We denote  $\mathbf{p}_0$  and  $\mathbf{p}_1$  lifts of  $p_0$  and  $p_1$  to  $\mathbb{C}^3$ . In view of equation (2.1), if we normalize two vectors  $\mathbf{p}_0$  and  $\mathbf{p}_1$  so that  $\langle \mathbf{p}_0, \mathbf{p}_0 \rangle = \langle \mathbf{p}_1, \mathbf{p}_1 \rangle$ , the equation (2.2) of the bisector then becomes simply

$$(2.3) \quad |\langle u, \mathbf{p}_0 \rangle| = |\langle u, \mathbf{p}_1 \rangle|.$$

A bisector in  $\mathbf{H}_\mathbb{C}^2$  is a smooth codimension one real hypersurface diffeomorphic to a 3-ball, but it is not totally geodesic. The *spinal sphere* of the bisector  $\mathcal{B}(p_0, p_1)$  is the ideal boundary of it on  $\partial\mathbf{H}_\mathbb{C}^2$ . The *complex spine* of the bisector  $\mathcal{B}(p_0, p_1)$  is by definition the complex geodesic that contains  $p_0$  and  $p_1$ . The *real spine* is a real geodesic in the complex spine that is equidistant between  $p_0$  and  $p_1$ .

There is a natural extension of the real spine to projective space, given by the (not necessarily negative) vectors in  $\text{Span}_{\mathbb{C}}(\mathbf{p}_0, \mathbf{p}_1)$  satisfying equation (2.3). We call this the *extended real spine* of the bisector.

Although bisector  $\mathcal{B}$  is not totally geodesic, it can be described in two different ways in terms of a foliation by totally geodesic subspaces.  $\mathcal{B}$  is the preimage of the real spine under the orthogonal projection onto the complex spine; each complex line that is the preimage of a point of the real spine is called a *complex slice* of  $\mathcal{B}$ .  $\mathcal{B}$  is also the union of all Lagrangian planes that contain the real spine; each Lagrangian plane is called a *real slice* of  $\mathcal{B}$ .

We will describe bisectors by giving two points on their extended real spines. In fact, we can describe a real geodesic as the projectivization of a totally real 2-dimensional subspace of  $\mathbb{C}^{2,1}$ , i.e. we take two vectors  $u$  and  $v$  in  $\mathbb{C}^3$  with  $\langle u, v \rangle \in \mathbb{R}$ , and consider their real span. The simplest way to guarantee that the span really yields a geodesic in  $\mathbf{H}_{\mathbb{C}}^2$  is to require moreover that  $v$  and  $u$  form a Lorentz basis, i.e.  $\langle v, v \rangle = -1$ ,  $\langle u, u \rangle = 1$  and  $\langle v, u \rangle = 0$ .

Let  $\Sigma_1$  and  $\Sigma_2$  be the complex spines of the bisectors  $\mathcal{B}_1$  and  $\mathcal{B}_2$ , and let  $\sigma_1$  and  $\sigma_2$  be their real spines. Then  $\Sigma_1$  and  $\Sigma_2$  coincide, or they intersect at a single point. Note that if  $\Sigma_1$  and  $\Sigma_2$  intersect outside the real spines  $\sigma_1$  and  $\sigma_2$ , then  $\mathcal{B}_1 \cap \mathcal{B}_2$  can be written as the equidistant locus from three points in general position.

First, we assume that the bisectors  $\mathcal{B}_1$  and  $\mathcal{B}_2$  have the same complex spine.

**Definition 2.4.** The bisectors  $\mathcal{B}_1$  and  $\mathcal{B}_2$  are called *cospinal* if and only if their complex spines  $\Sigma_1$  and  $\Sigma_2$  coincide.

In this case, it follows from the slice decomposition that  $\mathcal{B}_1 \cap \mathcal{B}_2$  is non-empty if and only if their real spines  $\sigma_1$  and  $\sigma_2$  intersect at a point  $p \in \mathbf{H}_{\mathbb{C}}^2$ . Moreover,  $\mathcal{B}_1 \cap \mathcal{B}_2$  consists of a complex geodesic  $\mathcal{S}$ , namely the complex geodesic orthogonal to  $\Sigma_1 = \Sigma_2$  through the point  $p$ .

Furthermore, we can describe the intersection of  $\mathcal{S}$  with another bisector  $\mathcal{B}_3(p_0, p_3)$  as follows, see [5].

We can choose a basis  $\{v_1, v_2\}$  for  $\mathcal{S}$ , with  $\langle v_1, v_2 \rangle = 0$ ,  $\langle v_1, v_1 \rangle = -1$ , and  $\langle v_2, v_2 \rangle = 1$ . Then the vectors in  $\mathcal{S}$  can be parameterized as

$$(2.4) \quad \mathcal{S} = \{v_1 + zv_2 : |z| < 1\}.$$

The intersection  $\mathcal{S} \cap \mathcal{B}_3(p_0, p_3)$  with a third bisector has an equation of the form

$$(2.5) \quad |\langle v_1 + zv_2, p_0 \rangle| = |\langle v_1 + zv_2, p_3 \rangle|,$$

which is a circle (or Euclidean line) in the  $z$ -plane.

In particular, the intersection of  $\mathcal{S}$  with a number of half spaces in  $\mathbf{H}_{\mathbb{C}}^2$  is bounded by circles or lines in the unit disk. One should be aware that such an intersection need not be connected in general, since the arcs of circles bounding it are not necessarily geodesic.

Now suppose  $\Sigma_1$  and  $\Sigma_2$  are distinct complex spines of  $\mathcal{B}_1$  and  $\mathcal{B}_2$  respectively. We call  $\mathcal{B}_1$  and  $\mathcal{B}_2$  *coequidistant* if and only if  $\Sigma_1$  and  $\Sigma_2$  intersect outside the real spines. The following result is due to Giraud, see [9], which is crucial to the study of Dirichlet domain.

**Proposition 2.5.** *Let  $p_0, p_1$  and  $p_2$  be distinct points in  $\mathbf{H}_{\mathbb{C}}^2$ , not all contained in a complex line. When it is non-empty, the intersection  $\mathcal{B}(p_0, p_1) \cap \mathcal{B}(p_0, p_2)$  is a (non-totally geodesic) smooth disk. Moreover, it is contained in precisely three bisectors, namely  $\mathcal{B}(p_0, p_1)$ ,  $\mathcal{B}(p_0, p_2)$  and  $\mathcal{B}(p_1, p_2)$ .*

**Definition 2.6.** The intersection of two coequidistant bisectors with distinct complex spines is called *Giraud disk*.

In order to find the combinatorics of the Dirichlet domain, we must determine the intersection of the bisectors. Unlike in real hyperbolic space, the intersection of two bisectors is not necessarily connected, see [9] for the details. Due to Proposition 2.5, we choose the bisectors bounding a Dirichlet domain  $D$  to form a very special family of bisectors; namely, they are all equidistant from a given point  $p_0$ .

We will review a convenient way to parametrize a Giraud disk, see [6, 7]. Consider two coequidistant bisectors  $\mathcal{B}_1(p_0, p_1)$  and  $\mathcal{B}_2(p_0, p_2)$ , which we assume not to be coplanar.

Let  $\mathbf{p}_j$  denote a lift of  $p_j$  to  $\mathbb{C}^3$ . We may assume that the three square norms  $\langle \mathbf{p}_j, \mathbf{p}_j \rangle$  are equal up to the rescaling. We also assume  $\langle \mathbf{p}_0, \mathbf{p}_1 \rangle$  and  $\langle \mathbf{p}_0, \mathbf{p}_2 \rangle$  are real and positive.

Define  $\tilde{v}_j = \mathbf{p}_0 - \mathbf{p}_j$  and  $\tilde{w}_j = i(\mathbf{p}_0 + \mathbf{p}_j)$  for  $j = 1, 2$ . We can normalize these to unit vectors  $v_j = \tilde{v}_j / \sqrt{-\langle \tilde{v}_j, \tilde{v}_j \rangle}$  and  $w_j = \tilde{w}_j / \sqrt{\langle \tilde{w}_j, \tilde{w}_j \rangle}$ . Then  $\tilde{v}_j$  is the midpoint of the geodesic segment between  $p_0$  and  $p_j$ . The extended real spine of  $\mathcal{B}_j(p_0, p_j)$  can be parametrized as the (not necessarily negative) vectors of the form  $w_j + tv_j$  ( $t \in \mathbb{R}$ ). Thus the intersection  $\mathcal{B}_1 \cap \mathcal{B}_2$  is given by negative vectors of the form

$$V(t_1, t_2) = (w_1 + t_1 v_1) \boxtimes (w_2 + t_2 v_2),$$

with  $t_1, t_2 \in \mathbb{R}$ . Its extension to projective space will be called *Giraud torus*, i.e., the vector  $V(t_1, t_2)$  is no longer required to have a negative square norm, we often denote it by  $\widehat{\mathcal{B}}_1 \cap \widehat{\mathcal{B}}_2$ . With the parameterization of the extended real spine of  $\mathcal{B}_j$ , it is evident that point  $v_j$  is missing. But the projectivization of the orthogonal complement of  $v_j$  ( $j = 1, 2$ ) does not intersect  $\mathbf{H}_{\mathbb{C}}^2$ . Given three points  $p_0, p_1$  and  $p_2$ , it is easy to determine whether the intersection  $\mathcal{B}_1(p_0, p_1) \cap \mathcal{B}_2(p_0, p_2)$  is empty or not by finding a sample point. Note that the condition  $\langle V(t_1, t_2), V(t_1, t_2) \rangle$  is negative is equivalent to

$$(2.6) \quad \det \begin{bmatrix} \langle w_1 + t_1 v_1, w_1 + t_1 v_1 \rangle & \langle w_1 + t_1 v_1, w_2 + t_2 v_2 \rangle \\ \langle w_2 + t_2 v_2, w_1 + t_1 v_1 \rangle & \langle w_2 + t_2 v_2, w_2 + t_2 v_2 \rangle \end{bmatrix} > 0.$$

### 3. THE REPRESENTATION AND THE GROUP

In her Ph.D thesis [11], Granier constructed a convex-compact representation  $\rho$  of the polygon-group  $G_{6,3}$  in  $\mathbf{PU}(2, 1)$ . She constructed a Dirichlet domain for  $\rho(G_{6,3})$  and proved that  $\rho(G_{6,3})$  is discrete by using Poincaré polyhedron theorem in  $\mathbf{H}_{\mathbb{C}}^2$ .

**Definition 3.1.** Fix two natural numbers  $p \geq 5$  and  $q \geq 3$ . The *polygon-group* is defined as follows

$$(3.1) \quad G_{p,q} = \langle a_0, a_1, \dots, a_{p-1} | a_i^q = [a_i, a_{i+1}] = id, i \in \mathbb{Z}/p\mathbb{Z} \rangle.$$

Let

$$(3.2) \quad H_{p,q} = \langle a_0, r | a_0^q = r^p = [a_0, r a_0 r^{-1}] = id \rangle$$

be another group. Let  $\phi : H_{p,q} \rightarrow \mathbb{Z}_p$  be the group homomorphism defined by  $\phi(a_0) = 0$  and  $\phi(r) = 1$ . Then  $G_{p,q}$  is the kernel of  $\phi$ . This shows that  $G_{p,q}$  is a normal subgroup of  $H_{p,q}$  of index  $p$ . We owe this observation to one of the referees.

We now review the representation  $\rho$  of  $G_{6,3}$  in [11]. In fact, Granier gave the representation  $\rho : H_{6,3} \rightarrow \mathbf{PU}(2, 1)$ . We will use the first model for the complex

hyperbolic plane in Section 2. Consider a regular right-angled  $p$ -gon  $\mathcal{P}$  in a well-chosen real hyperbolic plane  $\mathbf{H}_{\mathbb{R}}^2 \subset \mathbf{H}_{\mathbb{C}}^2$  with vertices  $x_j$  for  $j = 0, 1, \dots, p-1$ . The center of  $\mathcal{P}$  is located at  $o = (1, 0, 0)^t$ . The lift of  $x_j$  is given as

$$x_j = \begin{pmatrix} 1 \\ s \cdot \cos(\frac{2j\pi}{p}) \\ s \cdot \sin(\frac{2j\pi}{p}) \end{pmatrix},$$

where

$$s = \frac{\sqrt{2 \cos^2(\frac{2\pi}{p}) + 2 \cos(\frac{2\pi}{p})}}{1 + \cos(\frac{2\pi}{p})},$$

which is the Euclidean distance between the origin  $o$  and  $x_j$ . The Euclidean distance  $s$  is related to the complex hyperbolic distance  $d(o, x_j)$  by

$$s = \tanh\left(\frac{d(o, x_j)}{2}\right),$$

from which it follows

$$d(o, x_j) = 2 \operatorname{arccosh}\left(\frac{1 + \cos(2\pi/p)}{\sin(2\pi/p)}\right).$$

For  $0 \leq j \leq p-1$ , the geodesic side  $[x_j, x_{j+1}]$  of  $\mathcal{P}$  determines a complex geodesic  $C_j$  with polar vector  $e_j = x_j \boxtimes x_{j+1}$ . For example, one can get

$$e_0 = \begin{pmatrix} \sqrt{2 \cos^2(2\pi/p) + 2 \cos(2\pi/p)} \\ 1 + \cos(2\pi/p) \\ \sin(2\pi/p) \end{pmatrix}.$$

Let  $\gamma_j$  be the complex reflection of order  $q$  with mirror  $C_j$  and let

$$R_p = \begin{bmatrix} 1 & 0 & 0 \\ 0 & \cos(2\pi/p) & -\sin(2\pi/p) \\ 0 & \sin(2\pi/p) & \cos(2\pi/p) \end{bmatrix}.$$

We see that  $R_p(x_j) = x_{j+1}$  and the polygon  $\mathcal{P}$  is preserved by the rotation  $R_p$ . It follows that  $R_p(C_j) = C_{j+1}$  and  $\gamma_j = R_p^j \gamma_0 R_p^{-j}$ . We define  $\rho$  by the map  $\rho(a_j) = \gamma_j$  and  $\rho(r) = R_p$ .

When  $p = 6$  and  $q = 3$ , we have

$$R_6 = \begin{bmatrix} 1 & 0 & 0 \\ 0 & \frac{1}{2} & -\frac{\sqrt{3}}{2} \\ 0 & \frac{\sqrt{3}}{2} & \frac{1}{2} \end{bmatrix}$$

and

$$\gamma_0 = \begin{bmatrix} \frac{5}{2} - i\frac{\sqrt{3}}{2} & -\frac{3\sqrt{6}}{4} + i\frac{3\sqrt{2}}{4} & -\frac{3\sqrt{2}}{4} + i\frac{\sqrt{6}}{4} \\ \frac{3\sqrt{6}}{4} - i\frac{3\sqrt{2}}{4} & -\frac{5}{4} + i\frac{3\sqrt{3}}{4} & -\frac{3\sqrt{3}}{4} + \frac{3}{4}i \\ \frac{3\sqrt{2}}{4} - i\frac{\sqrt{6}}{4} & -\frac{3\sqrt{3}}{4} + \frac{3}{4}i & \frac{1}{4} + i\frac{\sqrt{3}}{4} \end{bmatrix}.$$

Since the polar vectors  $e_j$  and  $e_{j+1}$  are orthogonal, we have  $\gamma_i \gamma_{i+1} = \gamma_{i+1} \gamma_i$ . Subsequently, we often write  $\Gamma$  instead of  $\rho(G_{6,3})$ .



## 4. DIRICHLET DOMAIN OF THE GROUP

Given any group  $G$  acting on  $\mathbf{H}_{\mathbb{C}}^2$ , the Dirichlet domain centered at  $p_0 \in \mathbf{H}_{\mathbb{C}}^2$  is by definition

$$D = D_G = \{u \in \mathbf{H}_{\mathbb{C}}^2 : d(u, p_0) \leq d(u, \gamma(p_0)), \forall \gamma \in G\}.$$

The group  $G$  acts discretely if and only if  $D$  has nonempty interior, and in that case,  $D_G$  is a fundamental domain for  $G$  as long as no element of the group fixes the point  $p_0$ . If  $p_0$  is fixed by some non-trivial element of  $G$ , then one only gets a fundamental domain modulo the action of the finite group that fixes  $p_0$ .

Note that  $R_6$  is a regular elliptic element of order 6, with isolated fixed point at  $o = (1, 0, 0)^t$ . The point  $o$  will be chosen as the center of the Dirichlet domain of  $\Gamma$ .

One wishes the Dirichlet domain of  $\Gamma$  has only finitely many faces that are on bisectors, so that we can first consider the *partial Dirichlet domain*

$$D_S = \{u \in \mathbf{H}_{\mathbb{C}}^2 : d(u, p_0) \leq d(u, \gamma(p_0)), \forall \gamma \in S\}$$

for some finite subset  $S \subset \Gamma$ . Then  $D_S$  will be a priori domain larger than  $D_{\Gamma}$  by taking into account only the faces coming from  $S$  rather than all of  $\Gamma$ .

In order to ensure that  $D_S$  has side pairings, the generating set  $S$  should be symmetric, that is,  $S$  is closed under the operation of taking inverses in the group. For the group  $\Gamma = \rho(G_{6,3})$ , one can guess a reasonable candidates for the set  $S$ , which is the following set of 24 group elements:

$$S = \{\gamma_i, \gamma_i^{-1}, \gamma_i \gamma_{i+1}^{-1}, \gamma_{i+1} \gamma_i^{-1}, i \in \mathbb{Z}/6\mathbb{Z}\}.$$

Consider the partial Dirichlet domain  $D_S$ . For a given  $\gamma \in S$ , note that the intersection  $D_S \cap \mathcal{B}(o, \gamma(o))$  may be very complicated. When  $D_S \cap \mathcal{B}(o, \gamma(o))$  has a nonempty interior in  $\mathcal{B}(o, \gamma(o))$ , the face of  $D_S$  associated to the element  $\gamma$  is given by the connected components of  $D_S \cap \mathcal{B}(o, \gamma(o))$ , which is often denoted by  $b(o, \gamma(o))$ .

The main result of [11] is the following.

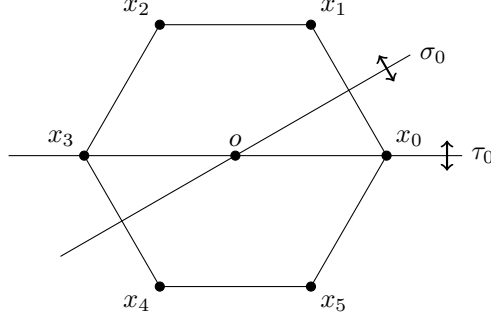
**Theorem 4.1.** *The Dirichlet domain  $D_{\Gamma}$  centered at  $o$  is equal to  $D_S$ . In particular,  $D_{\Gamma}$  has precisely 24 faces, namely the faces of  $D_{\Gamma}$  associated to the elements of  $S$ .*

In order to prove that  $D_S$  is a fundamental domain  $D_{\Gamma}$  of  $\Gamma$ , one should start by determining the precise combinatorics of  $D_S$ , then check the conditions of the Poincaré polyhedron theorem.

Note that  $D_S$  is a fundamental domain of  $\rho(G_{6,3})$ , but it is not a fundamental domain of  $\rho(H_{6,3})$ . In fact, since the element  $R_6$  fixes the center of  $D_S$  and preserve the  $D_S$  from the construction,  $D_S$  is a fundamental domain for the coset decomposition of  $\rho(H_{6,3})$  into left cosets of the cyclic group  $\langle R_6 \rangle$ .

For convenience, we write  $\mathcal{B}_k$ ,  $i = 0, 1, \dots, 11$ , for the bisectors bounding  $D_S$ , and  $b_k$ ,  $i = 0, 1, \dots, 11$ , for the intersection  $\mathcal{B}_k \cap D_S$ . See Table 1 for the notations. We also write  $\overline{\mathcal{B}_k}, \overline{b_k}$  for the bisectors and faces that associate to the inverse of the elements which associate to the  $\mathcal{B}_k$  and  $b_k$ . For example,  $\mathcal{B}_0 = \mathcal{B}(o, \gamma_0(o))$  and  $\overline{\mathcal{B}_0} = \mathcal{B}(o, \gamma_0^{-1}(o))$ . For each  $k$ , we denote  $\overline{\mathcal{B}_k}, \overline{\mathcal{B}_{\bar{k}}}$  and  $\overline{b_k}, \overline{b_{\bar{k}}}$  be their closures in  $\overline{\mathbf{H}_{\mathbb{C}}^2} = \mathbf{H}_{\mathbb{C}}^2 \cup \partial\mathbf{H}_{\mathbb{C}}^2$ .

We next describe the symmetry of  $D_S$ . From the construction,  $D_S$  is  $R_6$ -invariant. It has at most 2 isometry types of faces, that is, each face is isometric

FIGURE 1. The polygon  $\mathcal{P}$  and its symmetry.

to the face on  $\mathcal{B}_0$  or  $\mathcal{B}_6$ . In [11], Granier also observed that there are two complex reflections preserving  $D_S$ .

Let  $\tau_0, \sigma_0 : \mathbb{C}^3 \rightarrow \mathbb{C}^3$  be given as follows:

$$\tau_0 : \begin{pmatrix} z_1 \\ z_2 \\ z_3 \end{pmatrix} \mapsto \begin{pmatrix} z_1 \\ z_2 \\ -z_3 \end{pmatrix}$$

and

$$\sigma_0 : \begin{pmatrix} z_1 \\ z_2 \\ z_3 \end{pmatrix} \mapsto \begin{pmatrix} z_1 \\ z_2 \cos(\frac{2\pi}{6}) + z_3 \sin(\frac{2\pi}{6}) \\ z_2 \sin(\frac{2\pi}{6}) - z_3 \cos(\frac{2\pi}{6}) \end{pmatrix}.$$

Then we have

- $\tau_0$  fixes the vertices  $x_0$  and  $x_3$ , which also interchanges two pair of vertices  $\{x_1, x_5\}$  and  $\{x_2, x_4\}$ ;
- $\tau_0 \gamma_k \tau_0 = \gamma_{5-k}$  for  $k = 0 \dots, 5$ , therefore,  $\tau_0(\mathcal{B}_k) = \mathcal{B}_{5-k}$  for  $k = 0 \dots, 5$ ;  $\tau_0(\mathcal{B}_k) = \mathcal{B}_{\overline{16-k}}$  for  $k = 6 \dots, 10$  and  $\tau_0(\mathcal{B}_{11}) = \mathcal{B}_{\overline{11}}$ ;
- $\sigma_0$  interchanges three pair of vertices  $\{x_0, x_1\}$ ,  $\{x_2, x_5\}$  and  $\{x_3, x_4\}$ ;
- $\sigma_0 \gamma_0 \sigma_0 = \gamma_0$ ,  $\sigma_0 \gamma_k \sigma_0 = \gamma_{6-k}$  for  $k = 1, 2, 3, 4, 5$ , therefore,  $\sigma_0(\mathcal{B}_0) = \mathcal{B}_0$ ;  $\sigma_0(\mathcal{B}_k) = \mathcal{B}_{6-k}$  for  $k = 1, 2, 3, 4, 5$ ;  $\sigma_0(\mathcal{B}_{\overline{0}}) = \mathcal{B}_{\overline{0}}$ ,  $\sigma_0(\mathcal{B}_{\overline{k}}) = \mathcal{B}_{\overline{6-k}}$  for  $k = 1, 2, 3, 4, 5$ ;  $\sigma_0(\mathcal{B}_k) = \mathcal{B}_{\overline{17-k}}$  for  $k = 6, \dots, 11$ . See Figure 1.

Define  $\tau_j = R_6^j \tau_0 R_6^{-j}$  and  $\sigma_j = R_6^j \sigma_0 R_6^{-j}$ . It is easy to see that these isometries also preserve  $D_S$ .

**4.1. The combinatorics of  $D_S$ .** We now describe the combinatorics of  $D_S$  following [11] in details. By the symmetry of  $D_S$ , it is enough to determine the combinatorics of two faces of  $D_S$ , namely,  $\mathcal{B}_0 \cap D_S$  and  $\mathcal{B}_6 \cap D_S$ . Since any two of these 24 bisectors bounding  $D_S$  are coequidistant, their pairwise intersection is diffeomorphic to a disk, which is either a Giraud disk or a complex geodesic.

The following two lemmas give the details of the intersections of  $\mathcal{B}_0$  with the other 23 bisectors.

**Lemma 4.2.**  $\mathcal{B}_0$  intersects exactly 9 bisectors of the 23 other bisectors, that is,  $\mathcal{B}_{\overline{0}}$ ,  $\mathcal{B}_1$ ,  $\mathcal{B}_{\overline{1}}$ ,  $\mathcal{B}_5$ ,  $\mathcal{B}_{\overline{5}}$ ,  $\mathcal{B}_6$ ,  $\mathcal{B}_{\overline{6}}$ ,  $\mathcal{B}_{11}$  and  $\mathcal{B}_{\overline{11}}$ . The intersection  $\mathcal{B}_0 \cap \mathcal{B}_{\overline{0}}$  is a complex geodesic and the other corresponding intersections are all Giraud disks.

TABLE 1. The notations for the bisectors associated with  $D_S$ .

Element of $S$	Bisector
$\gamma_0$	$\mathcal{B}_0 = \mathcal{B}(o, \gamma_0(o))$
$\gamma_1$	$\mathcal{B}_1 = R_6(\mathcal{B}_0)$
$\gamma_2$	$\mathcal{B}_2 = R_6^2(\mathcal{B}_0)$
$\gamma_3$	$\mathcal{B}_3 = R_6^3(\mathcal{B}_0)$
$\gamma_4$	$\mathcal{B}_4 = R_6^4(\mathcal{B}_0)$
$\gamma_5$	$\mathcal{B}_5 = R_6^5(\mathcal{B}_0)$
$\gamma_0\gamma_1^{-1}$	$\mathcal{B}_6 = \mathcal{B}(o, \gamma_0\gamma_1^{-1}(o))$
$\gamma_1\gamma_2^{-1}$	$\mathcal{B}_7 = R_6(\mathcal{B}_6)$
$\gamma_2\gamma_3^{-1}$	$\mathcal{B}_8 = R_6^2(\mathcal{B}_6)$
$\gamma_3\gamma_4^{-1}$	$\mathcal{B}_9 = R_6^3(\mathcal{B}_6)$
$\gamma_4\gamma_5^{-1}$	$\mathcal{B}_{10} = R_6^4(\mathcal{B}_6)$
$\gamma_5\gamma_0^{-1}$	$\mathcal{B}_{11} = R_6^5(\mathcal{B}_6)$

**Lemma 4.3.**  $\mathcal{B}_0 \cap \mathcal{B}_{\bar{1}} \cap D_S$ ,  $\mathcal{B}_0 \cap \mathcal{B}_{\bar{5}} \cap D_S$ ,  $\mathcal{B}_0 \cap \mathcal{B}_{\bar{6}} \cap D_S$  and  $\mathcal{B}_0 \cap \mathcal{B}_{\bar{11}} \cap D_S$  are empty set.

A 2-face of  $D_S$  is the 2-dimensional intersection of two faces of  $D_S$ . The precise combinatorics of each 2-face of  $b_0$  has been studied in detail in [11].

**Proposition 4.4.** *The closure  $\overline{b_0}$  of  $b_0$  in  $\mathbf{H}_{\mathbb{C}}^2 \cup \partial\mathbf{H}_{\mathbb{C}}^2$  has precisely six 2-faces, five finite ones and one on the spinal sphere associated to  $\mathcal{B}_0$ .*

- The finite 2-faces on the (closure of the) Giraud disks  $\overline{\mathcal{B}_0} \cap \overline{\mathcal{B}_1}$  and  $\overline{\mathcal{B}_0} \cap \overline{\mathcal{B}_5}$  are topological triangles, see Figure 2. In particular, the second 2-face is the image of the first 2-face under the action of the isometry  $\sigma_0$ .
- The finite 2-faces on the (closure of the) Giraud disks  $\overline{\mathcal{B}_0} \cap \overline{\mathcal{B}_6}$  and  $\overline{\mathcal{B}_0} \cap \overline{\mathcal{B}_{\bar{11}}}$  are topological triangles, see Figure 3. In particular, the second 2-face is the image of the first 2-face under the action of the isometry  $\sigma_0$ .
- The finite 2-face on the (closure of the) complex geodesic  $\overline{\mathcal{B}_0} \cap \overline{\mathcal{B}_{\bar{0}}}$  is a topological hexagon, see Figure 4.
- The 2-face on the spinal sphere  $\partial\mathcal{B}_0$  is a topological hexagon, see Figure 6 and Figure 13.

**Lemma 4.5.**  $\mathcal{B}_6$  intersects exactly 7 bisectors of the other 23 bisectors, that is,  $\mathcal{B}_0$ ,  $\mathcal{B}_{\bar{0}}$ ,  $\mathcal{B}_1$ ,  $\mathcal{B}_{\bar{1}}$ ,  $\mathcal{B}_{\bar{6}}$ ,  $\mathcal{B}_{\bar{7}}$  and  $\mathcal{B}_{\bar{11}}$ . The corresponding intersections are all Giraud disks.

**Lemma 4.6.**  $\mathcal{B}_6 \cap \mathcal{B}_{\bar{0}} \cap D_S$ ,  $\mathcal{B}_6 \cap \mathcal{B}_1 \cap D_S$ ,  $\mathcal{B}_6 \cap \mathcal{B}_{\bar{6}} \cap D_S$ ,  $\mathcal{B}_6 \cap \mathcal{B}_{\bar{7}} \cap D_S$  and  $\mathcal{B}_6 \cap \mathcal{B}_{\bar{11}} \cap D_S$  are empty.

The precise combinatorics of each 2-face of  $b_6$  has also been studied in detail in [11].

**Proposition 4.7.** *The closure  $\overline{b_6}$  of  $b_6$  in  $\mathbf{H}_{\mathbb{C}}^2 \cup \partial\mathbf{H}_{\mathbb{C}}^2$  has precisely three 2-faces, two finite ones and one on the spinal sphere associated to  $\mathcal{B}_6$ .*

- The finite 2-faces on the (closure of the) Giraud disks  $\overline{\mathcal{B}_6} \cap \overline{\mathcal{B}_0}$  and  $\overline{\mathcal{B}_6} \cap \overline{\mathcal{B}_{\bar{1}}}$  are topological triangles, see Figure 5. In particular, the second 2-face is the image of the first 2-face under the action of the isometry  $\sigma_0$ .
- The 2-face on the spinal sphere  $\partial\mathcal{B}_6$  is a bigon, see Figure 7 and Figure 13.

By applying a version of Poincaré polyhedron theorem in the complex hyperbolic plane as stated for example in [22], [7] or [18], the main result obtained in [11] can be stated as follows.

**Theorem 4.8.** *Let  $D_S$  be defined as above, then  $D_S$  is a fundamental domain for  $\rho(G_{6,3})$ . Moreover,  $\Gamma = \rho(G_{6,3})$  is discrete and has the presentation*

$$\langle \gamma_0, \dots, \gamma_5 \mid \gamma_j^3 = id, \gamma_j \gamma_{j+1} = \gamma_{j+1} \gamma_j, j \in \mathbb{Z}/6\mathbb{Z} \rangle.$$

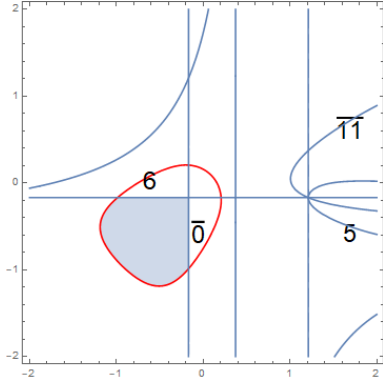


FIGURE 2. The 2-face of  $\bar{b}_0$  on the Giraud disk  $\bar{\mathcal{B}}_0 \cap \bar{\mathcal{B}}_1$ , which is bounded by the red Jordan curve. Here we write  $k$  for  $\mathcal{B}_k$  and  $\bar{k}$  for  $\bar{\mathcal{B}}_k$ .

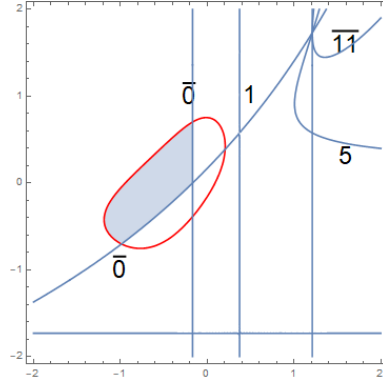


FIGURE 3. The 2-face of  $\bar{b}_0$  on the Giraud disk  $\bar{\mathcal{B}}_0 \cap \bar{\mathcal{B}}_6$ .

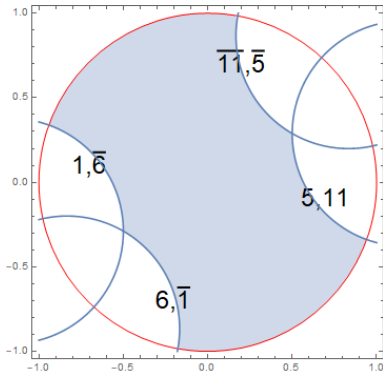


FIGURE 4. The 2-face of  $\bar{b}_0$  on the complex geodesic  $\bar{\mathcal{B}}_0 \cap \bar{\mathcal{B}}_0$ .

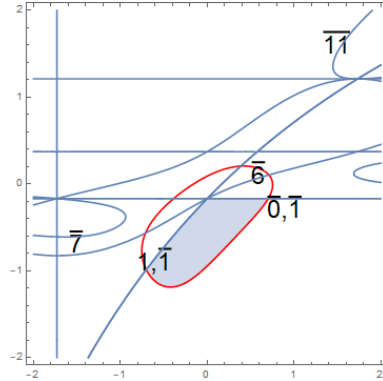


FIGURE 5. The 2-face of  $\bar{b}_6$  on the Giraud disk  $\bar{\mathcal{B}}_6 \cap \bar{\mathcal{B}}_0$ .

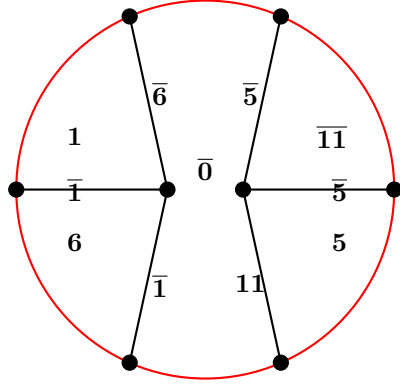


FIGURE 6. A schematic view of the combinatorics of the face of  $\bar{b}_0$ .

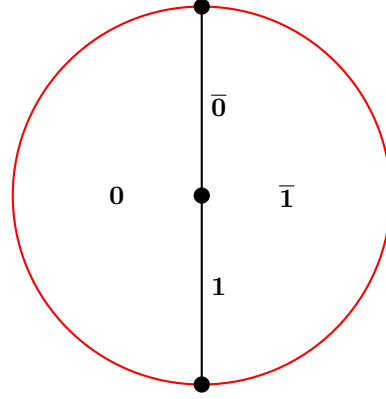


FIGURE 7. A schematic view of the combinatorics of the face of  $\bar{b}_6$ .

## 5. THE COMBINATORICS AT INFINITY OF THE DIRICHLET DOMAIN

The ideal boundary of a set  $X \subset \mathbf{H}_{\mathbb{C}}^2$  will be denoted by  $\partial_{\infty} X \subset \partial \mathbf{H}_{\mathbb{C}}^2$ . Let  $\Omega$  be the set of discontinuity of the discrete subgroup  $\rho(G_{6,3})$  acting on  $\partial \mathbf{H}_{\mathbb{C}}^2 = \mathbb{S}^3$ . In this section, we show  $\partial_{\infty} D_S \cap \Omega$  is a solid torus in the 3-sphere  $\partial \mathbf{H}_{\mathbb{C}}^2$ . The idea is to consider the intersection with  $\partial \mathbf{H}_{\mathbb{C}}^2$  of the fundamental domain  $D_S$  for the action on  $\mathbf{H}_{\mathbb{C}}^2$ . The main result in this section is Proposition 5.3, which is also the key for the proof of Theorem 1.2.

In what follows, the set  $\partial_{\infty} D_S$  will be denoted by  $T$ . Note that  $T$  is bounded by 24 pieces of spinal spheres. A realistic view of  $T$  is given in Figure 8, which is drawn in the boundary of Siegel model. So  $T$  is contained in the unbounded region bounded by the torus in Figure 8. From the analysis of the combinatorics of  $D_S$  given in the previous section, the combinatorial structure of  $\partial T$  can be seen in a schematic picture given in Figure 13. The picture is obtained by putting together the incidence information for each 2-face on these spinal spheres. One should keep this picture in mind for the gluing of these 24 faces.

**Proposition 5.1.**  *$\partial T$  is a torus.*

*Proof.* From the precise combinatorics of the 2-faces of  $b_0$  and  $b_6$  given in Propositions 4.4, 4.7, we can get Figure 13 by gluing together these 24 faces. The curves colored red and green are glued together, respectively. Thus we see that  $\partial T$  is a torus.  $\square$

The torus  $\partial T$  divides  $\mathbb{S}^3$  into two parts: outside (containing  $\infty$ ) and inside. The inside may be a solid torus and the outside a knot complement, or vice-versa, or both sides may be solid tori. J. W. Alexander's theorem tells us that  $\partial T$  in  $\mathbb{S}^3$  bounds a solid torus on at least one side, see [20]. In fact, in our case it seems  $\partial T$  bounds a solid torus on both side in  $\mathbb{S}^3$ . We just show  $T$  is a solid torus by producing an explicit simple closed curve which bounds a disk in  $T$ .

The main goal in our analysis is to produce an explicit embedded disk in  $T$  whose boundary is the red curve on the up and down side of Figure 13. This disk will

cut  $T$  into a 3-ball, then we can get the fundamental group of  $\Omega/\Gamma$  from the gluing maps.

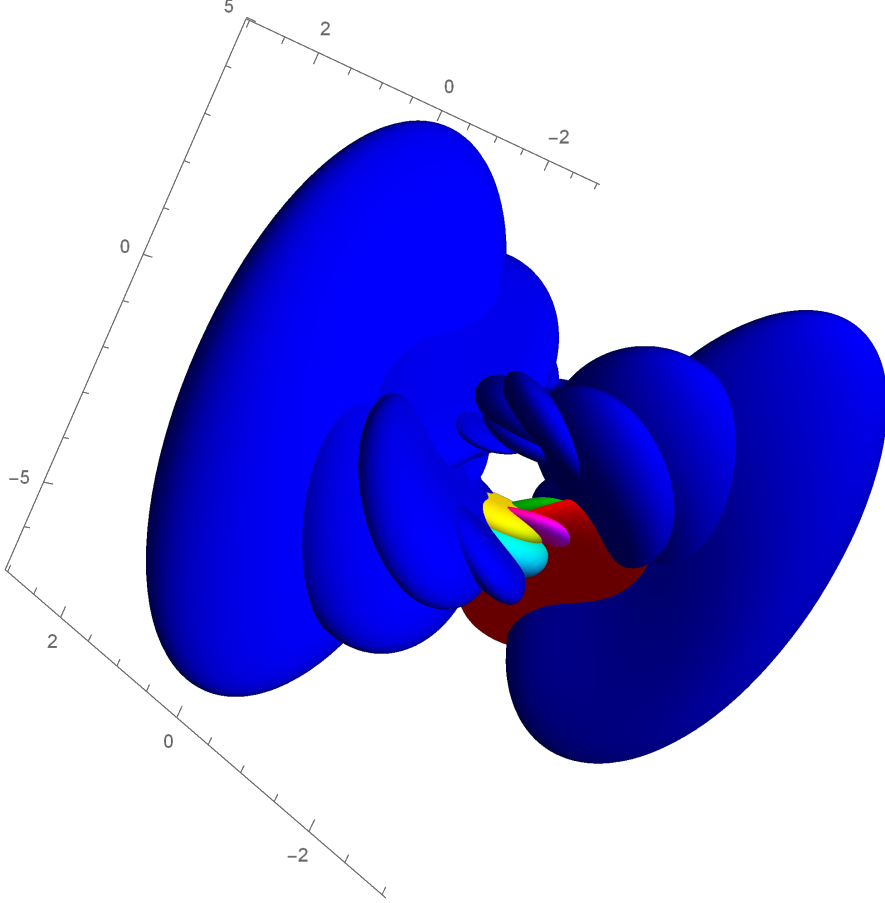


FIGURE 8. The solid torus  $T$  is drawn on the boundary of Siegel model. Where the red (resp. green, yellow, cyan, purple) sphere is the spinal sphere of  $\gamma_0$  (resp.  $\gamma_0^{-1}$ ,  $\gamma_1^{-1}$ ,  $\gamma_1$ ,  $\gamma_6$ ).

Let  $\mathcal{C}$  be the bisector  $\mathcal{B}(\gamma_1\gamma_0^{-1}(o), \gamma_0\gamma_1^{-1}(o))$ . Then one can show that

**Proposition 5.2.** *The bisector  $\mathcal{C}$  intersects with the 24 bisectors bounding  $D_S$ .*

*Proof.* We show that the intersection of the bisector  $\mathcal{C}$  with each bisector of the 24 bisectors is a smooth disk. The argument used here can be found in Appendix of [6]. In order to show that  $\mathcal{C} \cap \mathcal{B}_{\bar{0}}$  is a disk, we consider the parametrization of the Giraud torus  $\widehat{\mathcal{C}} \cap \widehat{\mathcal{B}}_{\bar{0}}$ . We only need to exhibit a single point  $p_{\bar{0}} \in \mathbf{H}_{\mathbb{C}}^2$  inside the Giraud torus. For example, the point  $p_{\bar{0}}$  has the following form

$$\begin{aligned} p_{\bar{0}} &= (\gamma_0\gamma_1^{-1}(o) - \gamma_1\gamma_0^{-1}(o)) \boxtimes (o - \gamma_0^{-1}(o)) \\ &= \left( \frac{-3\sqrt{3} - 9i}{2}, \frac{-3 - 3\sqrt{3}i}{2\sqrt{2}}, \frac{-3\sqrt{3} - 9i}{2\sqrt{2}} \right) \end{aligned}$$

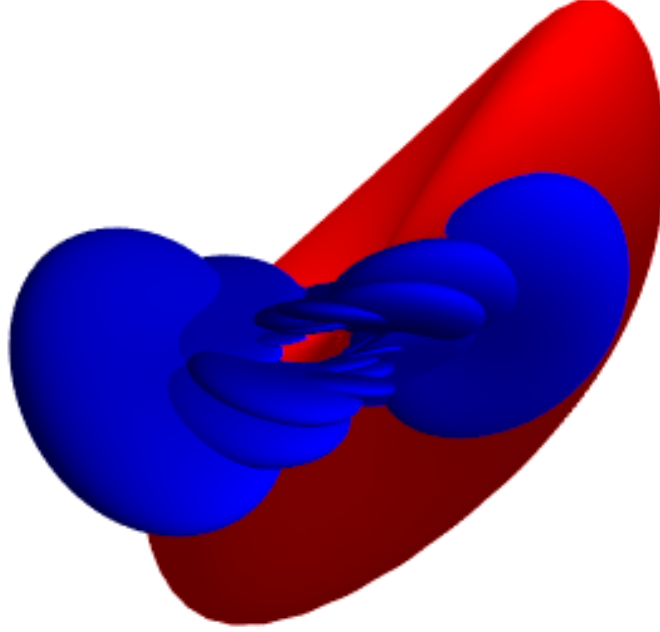


FIGURE 9. The solid torus  $T$  and the cutting disk on the spinal sphere of the bisector  $\mathcal{C}$ . We draw all the 24 spinal spheres for the set  $S$  in blue, and the spinal sphere of  $\mathcal{C}$  in Proposition 5.2 in red.  $T$  intersects this red sphere in two disks, one of which is our topological octagon  $\mathcal{E}$  in Proposition 5.3, which in turn implies  $T$  is a solid torus.

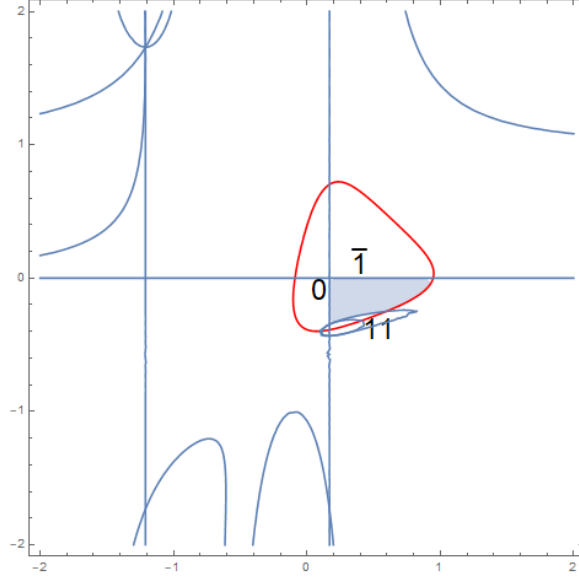
does the job, since  $\langle p_{\bar{0}}, p_{\bar{0}} \rangle = -9$ .

For the remainder cases, we just list the points and the corresponding Giraud tori. See Table 2.  $\square$

By using the techniques of Section 2, we can study the intersection of  $\mathcal{C}$  with each face of  $D_S$ . For example, the combinatorics of  $\mathcal{C} \cap \mathcal{B}_0 \cap D_S$  is shown in Figure 10. Then one can get the combinatorics of the intersection of the sphere  $\partial_\infty \mathcal{C}$  with the solid torus  $T$ . It can be seen that the interior of this intersection has two components, each of which is a topological octagon. Let  $\mathcal{E}$  be one of them. We will describe this octagon explicitly. The thick gray curve in Figure 13 in Section 6 is a schematic view of the boundary of  $\mathcal{E}$ . From which, it can be seen that  $\partial \mathcal{E}$  passes through the spinal spheres of  $\mathcal{B}_{\bar{0}}$ ,  $\mathcal{B}_{11}$ ,  $\mathcal{B}_5$ ,  $\mathcal{B}_4$ ,  $\mathcal{B}_3$ ,  $\mathcal{B}_2$ ,  $\mathcal{B}_{\bar{7}}$ , and  $\mathcal{B}_{\bar{1}}$  circularly.

Point	Giraud torus
$\left(\frac{-3\sqrt{3}+9i}{2}, \frac{-3+3\sqrt{3}i}{2\sqrt{2}}, \frac{-3\sqrt{3}+9i}{2\sqrt{2}}\right)$	$\widehat{\mathcal{C}} \cap \widehat{\mathcal{B}}_0, \widehat{\mathcal{C}} \cap \widehat{\mathcal{B}}_1, \widehat{\mathcal{C}} \cap \widehat{\mathcal{B}}_6, \widehat{\mathcal{C}} \cap \widehat{\mathcal{B}}_0, \widehat{\mathcal{C}} \cap \widehat{\mathcal{B}}_1, \widehat{\mathcal{C}} \cap \widehat{\mathcal{B}}_6$
$\left(\frac{3\sqrt{3}-9i}{2}, \frac{-3+3\sqrt{3}i}{2\sqrt{2}}, \frac{-3\sqrt{3}+9i}{2\sqrt{2}}\right)$	$\widehat{\mathcal{C}} \cap \widehat{\mathcal{B}}_3, \widehat{\mathcal{C}} \cap \widehat{\mathcal{B}}_4, \widehat{\mathcal{C}} \cap \widehat{\mathcal{B}}_9, \widehat{\mathcal{C}} \cap \widehat{\mathcal{B}}_3, \widehat{\mathcal{C}} \cap \widehat{\mathcal{B}}_4, \widehat{\mathcal{C}} \cap \widehat{\mathcal{B}}_9$
$\left(\frac{9\sqrt{3}-81i}{14}, \frac{-9+27\sqrt{3}i}{14\sqrt{2}}, \frac{9\sqrt{3}-81i}{14\sqrt{2}}\right)$	$\widehat{\mathcal{C}} \cap \widehat{\mathcal{B}}_2, \widehat{\mathcal{C}} \cap \widehat{\mathcal{B}}_7, \widehat{\mathcal{C}} \cap \widehat{\mathcal{B}}_2, \widehat{\mathcal{C}} \cap \widehat{\mathcal{B}}_7$
$\left(\frac{18\sqrt{3}-27i}{7}, \frac{18\sqrt{2}-9\sqrt{6}i}{7}, 0\right)$	$\widehat{\mathcal{C}} \cap \widehat{\mathcal{B}}_5, \widehat{\mathcal{C}} \cap \widehat{\mathcal{B}}_{11}, \widehat{\mathcal{C}} \cap \widehat{\mathcal{B}}_5, \widehat{\mathcal{C}} \cap \widehat{\mathcal{B}}_{11}$
$\left(\frac{-111\sqrt{3}-477i}{62}, \frac{111+159\sqrt{3}i}{31\sqrt{2}}, 0\right)$	$\widehat{\mathcal{C}} \cap \widehat{\mathcal{B}}_8, \widehat{\mathcal{C}} \cap \widehat{\mathcal{B}}_8$
$\left(\frac{111\sqrt{3}-477i}{62}, \frac{111-159\sqrt{3}i}{62\sqrt{2}}, \frac{-111\sqrt{3}+477i}{62\sqrt{2}}\right)$	$\widehat{\mathcal{C}} \cap \widehat{\mathcal{B}}_{10}, \widehat{\mathcal{C}} \cap \widehat{\mathcal{B}}_{10}$

TABLE 2. The point chosen inside each Giraud torus.

FIGURE 10. The combinatorics of  $\mathcal{C} \cap \widehat{\mathcal{B}}_0 \cap D_S$ . The ideal boundary of the intersection is an arc with endpoints on  $\partial_\infty \widehat{\mathcal{B}}_7$  and  $\partial_\infty \widehat{\mathcal{B}}_{11}$ .

We study the intersection of the closure of the bisectors with  $\partial_\infty \mathcal{C}$  by parametrizing  $\partial_\infty \mathcal{C}$ . In order to make the equation of these intersections having simple forms, we will choose the coordinates for  $\mathbf{H}_\mathbb{C}^2$  such that the midpoint of  $[\gamma_1 \gamma_0^{-1}(o), \gamma_0 \gamma_1^{-1}(o)]$  is at the origin. The coordinate transformation matrix is given by

$$P = \begin{bmatrix} 4\sqrt{\frac{2}{5}} & 0 & -3\sqrt{\frac{3}{5}}i \\ \frac{3}{2}\sqrt{\frac{3}{5}} & -\frac{\sqrt{3}}{2}i & -2\sqrt{\frac{2}{5}}i \\ \frac{9}{2\sqrt{5}} & \frac{i}{2} & -2\sqrt{\frac{6}{5}}i \end{bmatrix}.$$

We work in  $\mathbb{C}^2$ , with affine coordinates  $u_1 = \frac{z_1}{z_0}$ ,  $u_2 = \frac{z_2}{z_0}$ , where the  $z_j$  denote coordinates in the new Lorentz basis. The ball coordinates for  $\gamma_1 \gamma_0^{-1}(o)$  and  $\gamma_0 \gamma_1^{-1}(o)$



are given by  $(\pm\sqrt{\frac{3}{5}}, 0)$ , and the bisector  $\mathcal{C}$  has a very simple equation, namely

$$\operatorname{Re}(u_1) = 0.$$

So the bisector  $\mathcal{C}$  can simply be thought of as the unit ball in  $\mathbb{R}^3$ ,

$$\mathcal{C} = \{(it_3, t_1 + it_2) \in \mathbb{C}^2 \mid t_i \in \mathbb{R}, t_1^2 + t_2^2 + t_3^2 < 1\},$$

and  $\partial_\infty \mathcal{C}$  is the unit sphere.

The equation for the intersection of  $\mathcal{C}$  with the bisector  $\mathcal{B}(o, g(o))$  for some  $g$  has the form

$$|\langle Z, P^{-1}(p_0) \rangle| = |\langle Z, P^{-1}(g(p_0)) \rangle|,$$

where one takes  $Z = (1, it_3, t_1 + it_2)$ .

TABLE 3. The equations for the intersections of the eight bisectors with the bisector  $\mathcal{C}$ .

$\mathcal{B}_0$	$7 + 12t_1^2 + 12t_2^2 + 6\sqrt{5}t_3 - 5t_3^2 + 9\sqrt{6}t_2 + \sqrt{30}t_2t_3 - 5\sqrt{2}t_1 + 3\sqrt{10}t_1t_3$
$\mathcal{B}_{11}$	$113 + 78t_1^2 + 78t_2^2 - 60\sqrt{5}t_3 + 35t_3^2 + 20\sqrt{2}t_1 - 12\sqrt{10}t_1t_3 + 76\sqrt{6}t_2 - 20\sqrt{30}t_2t_3$
$\mathcal{B}_5$	$64 + 54t_1^2 + 54t_2^2 - 24\sqrt{5}t_3 + 3\sqrt{10}t_1t_3 + 10t_3^2 + 48\sqrt{6}t_2 - 9\sqrt{30}t_2t_3$
$\mathcal{B}_4$	$425 + 420t_1^2 + 420t_2^2 - 42\sqrt{5}t_3 + 5t_3^2 + 5\sqrt{2}t_1 + 3\sqrt{10}t_1t_3 + 345\sqrt{6}t_2 - 17\sqrt{30}t_2t_3$
$\mathcal{B}_3$	$425 + 420t_1^2 + 420t_2^2 + 42\sqrt{5}t_3 + 5t_3^2 + 5\sqrt{2}t_1 + 3\sqrt{10}t_1t_3 + 345\sqrt{6}t_2 + 17\sqrt{30}t_2t_3$
$\mathcal{B}_2$	$64 + 54t_1^2 + 54t_2^2 + 24\sqrt{5}t_3 - 3\sqrt{10}t_1t_3 + 10t_3^2 + 48\sqrt{6}t_2 + 9\sqrt{30}t_2t_3$
$\mathcal{B}_7$	$113 + 78t_1^2 + 78t_2^2 + 60\sqrt{5}t_3 + 35t_3^2 + 20\sqrt{2}t_1 + 12\sqrt{10}t_1t_3 + 76\sqrt{6}t_2 + 20\sqrt{30}t_2t_3$
$\mathcal{B}_1$	$-7 - 12t_1^2 - 12t_2^2 + 6\sqrt{5}t_3 + 5t_3^2 - 9\sqrt{6}t_2 + \sqrt{30}t_2t_3 + 5\sqrt{2}t_1 + 3\sqrt{10}t_1t_3$

TABLE 4. The boundary arcs of the octagon  $\mathcal{E}$ , which is the thick gray curve in Figure 13 of Section 6.

arc	Giraud disk	end points
$\alpha_1$	$\partial_\infty(\mathcal{C} \cap \mathcal{B}_0)$	$\partial_\infty(\mathcal{C} \cap \mathcal{B}_0) \cap \partial_\infty \mathcal{B}_1, \partial_\infty(\mathcal{C} \cap \mathcal{B}_0) \cap \partial_\infty \mathcal{B}_{11}$
$\alpha_2$	$\partial_\infty(\mathcal{C} \cap \mathcal{B}_{11})$	$\partial_\infty(\mathcal{C} \cap \mathcal{B}_{11}) \cap \partial_\infty \mathcal{B}_0, \partial_\infty(\mathcal{C} \cap \mathcal{B}_{11}) \cap \partial_\infty \mathcal{B}_5$
$\alpha_3$	$\partial_\infty(\mathcal{C} \cap \mathcal{B}_5)$	$\partial_\infty(\mathcal{C} \cap \mathcal{B}_5) \cap \partial_\infty \mathcal{B}_{11}, \partial_\infty(\mathcal{C} \cap \mathcal{B}_5) \cap \partial_\infty \mathcal{B}_4$
$\alpha_4$	$\partial_\infty(\mathcal{C} \cap \mathcal{B}_4)$	$\partial_\infty(\mathcal{C} \cap \mathcal{B}_4) \cap \partial_\infty \mathcal{B}_5, \partial_\infty(\mathcal{C} \cap \mathcal{B}_4) \cap \partial_\infty \mathcal{B}_3$
$\alpha_5$	$\partial_\infty(\mathcal{C} \cap \mathcal{B}_3)$	$\partial_\infty(\mathcal{C} \cap \mathcal{B}_3) \cap \partial_\infty \mathcal{B}_4, \partial_\infty(\mathcal{C} \cap \mathcal{B}_3) \cap \partial_\infty \mathcal{B}_2$
$\alpha_6$	$\partial_\infty(\mathcal{C} \cap \mathcal{B}_2)$	$\partial_\infty(\mathcal{C} \cap \mathcal{B}_2) \cap \partial_\infty \mathcal{B}_3, \partial_\infty(\mathcal{C} \cap \mathcal{B}_2) \cap \partial_\infty \mathcal{B}_7$
$\alpha_7$	$\partial_\infty(\mathcal{C} \cap \mathcal{B}_7)$	$\partial_\infty(\mathcal{C} \cap \mathcal{B}_7) \cap \partial_\infty \mathcal{B}_2, \partial_\infty(\mathcal{C} \cap \mathcal{B}_7) \cap \partial_\infty \mathcal{B}_1$
$\alpha_8$	$\partial_\infty(\mathcal{C} \cap \mathcal{B}_1)$	$\partial_\infty(\mathcal{C} \cap \mathcal{B}_1) \cap \partial_\infty \mathcal{B}_7, \partial_\infty(\mathcal{C} \cap \mathcal{B}_1) \cap \partial_\infty \mathcal{B}_0$

The octagon  $\mathcal{E}$  is bounded by the eight segments on the intersections of  $\partial_\infty \mathcal{C}$  with the closure of the above eight bisectors. We denote by  $\alpha_1, \alpha_2, \alpha_3, \alpha_4, \alpha_5, \alpha_6, \alpha_7$  and  $\alpha_8$  the arcs on  $\partial_\infty(\mathcal{C} \cap \mathcal{B}_0), \partial_\infty(\mathcal{C} \cap \mathcal{B}_{11}), \partial_\infty(\mathcal{C} \cap \mathcal{B}_5), \partial_\infty(\mathcal{C} \cap \mathcal{B}_4), \partial_\infty(\mathcal{C} \cap \mathcal{B}_3), \partial_\infty(\mathcal{C} \cap \mathcal{B}_2), \partial_\infty(\mathcal{C} \cap \mathcal{B}_7)$  and  $\partial_\infty(\mathcal{C} \cap \mathcal{B}_1)$  respectively, see Table 4 for the arcs and the boundaries of these eight arcs. From the equations in Table 3 and the equation of  $\partial_\infty \mathcal{C}$ , one can deduce explicit parametrizations for the segments of  $\mathcal{E}$ .

(1). The resultant of the equation of  $\partial_\infty(\mathcal{C} \cap \mathcal{B}_0)$  and  $t_1^2 + t_2^2 + t_3^2 - 1$  with respect to  $t_1$  has degree 2 in  $t_2$ . Using the quadratic formula, we get

$$t_2 = \phi_1(t_3) = \frac{a_1(t_3) + \sqrt{b_1(t_3)}}{8(67 + 6\sqrt{5}t_3 + 15t_3^2)},$$

where

$$a_1(t) = -171\sqrt{6} - 73\sqrt{30}t + 123\sqrt{6}t^2 + 17\sqrt{30}t^3$$

and  $b_1(t) = 8750 - 19500\sqrt{5}t + 72250t^2 - 11400\sqrt{5}t^3 - 62750t^4 + 38580\sqrt{5}t^5 - 36810t^6$ .

One then takes

$$t_1 = -\sqrt{1 - \phi_1(t_3)^2 - t_3^2}.$$

This parametrization is well defined for  $t_3$  in the interval  $[0, 0.321084..]$  which corresponds to the segment on  $\partial_\infty(\mathcal{C} \cap \mathcal{B}_0)$  of  $\mathcal{E}$ . So we give a parametrization for the arc  $\alpha_1$ .

(2). The segment  $\alpha_2$  can be divided into two subsegments. We give a parametrization for each one. Let

$$t_2 = \phi_2(t_3) = \frac{a_2(t_3) - \sqrt{b_2(t_3)}}{32(271 - 150\sqrt{5}t_3 + 105t_3^2)},$$

and

$$t_2 = \phi'_2(t_3) = \frac{a_2(t_3) + \sqrt{b_2(t_3)}}{32(271 - 150\sqrt{5}t_3 + 105t_3^2)},$$

where

$$a_2(t) = -955\sqrt{2} + 873\sqrt{10}t - 685\sqrt{2}t^2 - 129\sqrt{10}t^3,$$

and  $b_2(t) = -2220150 + 9226020\sqrt{2}t - 73068690t^2 + 60093240\sqrt{5}t^3 - 130836474t^4 + 27959460\sqrt{5}t^5 - 11466750t^6$ . Then we take

$$\left[ -\sqrt{1 - \phi_2(t_3)^2 - t_3^2}, \phi_2(t_3), t_3 \right]$$

for  $t_3$  in the interval  $[0.242665.., 0.270392..]$  for the first subsegment of  $\alpha_2$  and

$$\left[ -\sqrt{1 - \phi'_2(t_3)^2 - t_3^2}, \phi'_2(t_3), t_3 \right]$$

for  $t_3$  in the interval  $[0.242665.., 0.321084..]$  for the second subsegment of  $\alpha_2$ . Note that  $\phi'_2(0.242665..) = \phi_2(0.242665..)$ .

(3). For  $\alpha_3$ , we get

$$t_2 = \phi_3(t_3) = \frac{a_3(t_3) - \sqrt{b_3(t_3)}}{12(192 - 72\sqrt{5}t_3 + 35t_3^2)},$$

where

$$a_3(t) = -944\sqrt{6} + 369\sqrt{30}t + 172\sqrt{6}t^2 - 66\sqrt{30}t^3,$$

$$b_3(t) = -250t^2 + 1200\sqrt{5}t^3 - 1500\sqrt{5}t^4 + 7680\sqrt{5}t^5 - 11140t^6.$$

Then we take

$$t_1 = -\sqrt{1 - \phi_3(t_3)^2 - t_3^2}.$$

This gives a parametrization for  $\alpha_3$  for  $t_3$  in the interval  $[0.171638.., 0.270392..]$ .

(4). For  $\alpha_4$ , we get

$$t_2 = \phi_4(t_3) = \frac{a_4(t_3) - \sqrt{b_4(t_3)}}{8(17855 - 1758\sqrt{5}t_3 + 219t_3^2)},$$

where

$$\begin{aligned} a_4(t) &= -58305\sqrt{6} + 5771\sqrt{30}t + 27921\sqrt{6}t^2 - 1411\sqrt{30}t^3, \\ b_4(t) &= 350 + 1740\sqrt{5}t - 17270t^2 + 42312\sqrt{5}t^3 + 17074t^4 - 306708\sqrt{5}t^5 - 651546t^6. \end{aligned}$$

Then we take

$$t_1 = -\sqrt{1 - \phi_4(t_3)^2 - t_3^2}.$$

This gives a parametrization for  $\alpha_4$  for  $t_3$  in the interval  $[0, 0.171638..]$ .

(5). For  $\alpha_5$ , we get

$$t_2 = \phi_5(t_3) = \frac{a_5(t_3) + \sqrt{b_5(t_3)}}{8(17855 - 1758\sqrt{5}t_3 + 219t_3^2)},$$

where

$$\begin{aligned} a_5(t) &= -58305\sqrt{6} - 5771\sqrt{30}t + 27921\sqrt{6}t^2 + 1411\sqrt{30}t^3, \\ b_5(t) &= 350 - 1740\sqrt{5}t - 17270t^2 - 42312\sqrt{5}t^3 + 17074t^4 + 306708\sqrt{5}t^5 - 651546t^6. \end{aligned}$$

Then we take

$$t_1 = -\sqrt{1 - \phi_5(t_3)^2 - t_3^2}.$$

This gives a parametrization for  $\alpha_5$  for  $t_3$  in the interval  $[-0.171638.., 0]$ .

(6). For  $\alpha_6$ , we get

$$t_2 = \phi_6(t_3) = \frac{a_6(t_3) + \sqrt{b_6(t_3)}}{12(192 + 72\sqrt{5}t_3 + 35t_3^2)},$$

where

$$\begin{aligned} a_6(t) &= -944\sqrt{6} - 369\sqrt{30}t + 172\sqrt{6}t^2 + 66\sqrt{30}t^3, \\ b_6(t) &= -250t_3^2 - 1200\sqrt{5}t^3 - 9500t^4 - 7680\sqrt{5}t^5 - 11140t^6. \end{aligned}$$

Then we take

$$t_1 = -\sqrt{1 - \phi_6(t_3)^2 - t_3^2}.$$

This gives a parametrization for  $\alpha_6$  for  $t_3$  in the interval  $[-0.270392.., -0.171638..]$ .

(7). For  $\alpha_7$ , there are two subsegments with one common end point. We give a parametrization for each one. Let

$$t_2 = \phi_7(t_3) = \frac{a_7(t_3) + \sqrt{b_7(t_3)}}{32(271 + 150\sqrt{5}t_3 + 105t_3^2)},$$

and

$$t_2 = \phi_7'(t_3) = \frac{a_7(t_3) - \sqrt{b_7(t_3)}}{32(271 + 150\sqrt{5}t_3 + 105t_3^2)},$$

where

$$a_7(t) = -3629\sqrt{6} - 2095\sqrt{30}t - 683\sqrt{6}t^3 + 215\sqrt{30}t^3,$$

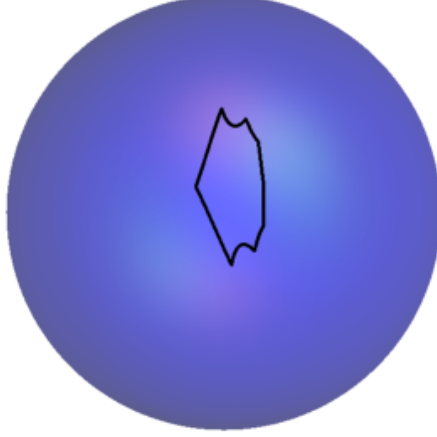


FIGURE 11. The cutting disk  $\mathcal{E}$  on  $\partial_\infty \mathcal{C} \simeq S^2$ , which is an octagon.

and  $b_7(t) = -51250 - 247500\sqrt{5}t - 2387750t^2 - 2452200\sqrt{5}t^3 - 7099550t^4 - 2180940\sqrt{5}t^5 - 1376010t^6$ .

Then we take

$$\left[ -\sqrt{1 - \phi_7(t_3)^2 - t_3^2}, \phi_7(t_3), t_3 \right]$$

for  $t_3$  in the interval  $[-0.321084.., -0.242665..]$  for the first part of  $\alpha_7$  and

$$\left[ -\sqrt{1 - \phi_7'(t_3)^2 - t_3^2}, \phi_7'(t_3), t_3 \right]$$

for  $t_3$  in the interval  $[-0.270392, -0.242665]$  for the second part of  $\alpha_7$ . Note that  $\phi_7(-0.242665..) = \phi_7'(-0.242665..)$ .

(8). For  $\alpha_8$ , we get

$$t_2 = \phi_8(t_3) = \frac{a_8(t_3) - \sqrt{b_8(t_3)}}{8(67 - 6\sqrt{5}t_3 + 15t_3^2)},$$

where

$$a_8(t) = -171\sqrt{6} + 73\sqrt{10}t + 123\sqrt{6}t^2 - 17\sqrt{30}t^3,$$

and  $b_8(t) = 8750 + 19500\sqrt{5}t + 72250t^2 + 11400\sqrt{5}t^3 - 62750t^4 - 38580\sqrt{5}t^5 - 36810t^6$ .

Then we take

$$t_1 = -\sqrt{1 - \phi_8(t_3)^2 - t_3^2}.$$

This gives a parametrization for  $\alpha_8$  for  $t_3$  in the interval  $[-0.321084.., 0]$ .

The curve  $\alpha = \bigcup_{i=1}^8 \alpha_i$  on  $\partial_\infty \mathcal{C} \simeq S^2$  bounds two disks, only one of which is completely contained in the half-sphere  $t_1 < 0$ . This is the cutting disk we need. See Figure 11.

We can show that the boundary curve  $\alpha$  of  $\mathcal{E}$  is embedded in  $\partial_\infty \mathcal{C}$  by solving a system of equations. For example, the equations  $\partial_\infty(\mathcal{C} \cap \mathcal{B}_0)$ ,  $\partial_\infty(\mathcal{C} \cap \mathcal{B}_{11})$  and

$t_1^2 + t_2^2 + t_3^2 - 1$  have two solutions

$$(-0.162508\dots, -0.933004\dots, 0.321084\dots), \quad (0.0546295\dots, -0.856302\dots, 0.513578\dots).$$

The point corresponding to the first solution is a vertex of  $\mathcal{E}$ . From the parametrization for  $\alpha_i$ , we know that the point corresponding to the second solution is not on the curve  $\alpha$ . Similar arguments apply to the intersections of the other pairs of arcs.

**Proposition 5.3.** *The topological octagon  $\mathcal{E}$  is properly contained in  $T$ .*

*Proof.* From the above construction, we see that points on the boundary of  $\mathcal{E}$  are precisely on the bisectors we think they are on, see Figure 11.

We now want to check that the closure of the eight bisectors and  $\partial_\infty \mathcal{C}$  have no unwanted extra intersection.

For example, it is possible that  $\mathcal{B}_0$  may have a connected component contained in the interior of  $\mathcal{E}$ . In this case, the restriction to  $\partial_\infty \mathcal{C}$  of the equation for  $\partial_\infty \mathcal{B}_0 \cap \partial_\infty \mathcal{C}$  would have a critical point in the interior of  $\mathcal{E}$ .

By using Lagrange multipliers, the critical points are the solutions of the system

$$\begin{cases} \nabla f = \lambda \nabla g, \\ g = 0, \end{cases}$$

where  $f$  is the equation for  $\partial_\infty \mathcal{B}_0 \cap \partial_\infty \mathcal{C}$  and  $g = t_1^2 + t_2^2 + t_3^2 - 1$ .

Then the system reads

$$\begin{cases} -5\sqrt{2} + 24t_1 - 2\lambda t_1 + 3\sqrt{10}t_3 = 0, \\ 9\sqrt{6} + 24t_2 - 2\lambda t_2 + \sqrt{30}t_3 = 0, \\ 6\sqrt{5} + 3\sqrt{10}t_1 + \sqrt{30}t_2 - 10t_3 - 2\lambda t_3 = 0, \\ t_1^2 + t_2^2 + t_3^2 - 1 = 0. \end{cases}$$

Solving the system by standard Groebner basis techniques, we get two solutions which are given approximately

$$(t_1, t_2, t_3) = (-0.173625, 0.942177, 0.286631), \quad (0.308076, -0.341632, -0.887906).$$

One can check that the points correspond to these two solutions are not in the interior of  $\mathcal{E}$ . See Figure 12, it is also clearly that the critical points of the equations are outside  $\mathcal{E}$ .

The analysis for the other intersections are similar, we omit the details. This ends the proof of Proposition 5.3.  $\square$

## 6. THE 3-ORBIFOLD AT INFINITY OF $\rho(G_{6,3})$

In this section, based on results in Section 5, we study the quotient of the domain of discontinuity under the action of the group  $\rho(G_{6,3})$  and identify the 3-orbifold  $\mathcal{O}$  at infinity of  $\mathbf{H}_{\mathbb{C}}^2/\rho(G_{6,3})$ . We also show  $\mathcal{O}$  is a closed hyperbolic 3-orbifold.

**6.1. The 3-orbifold  $\mathcal{O}$  at infinity of  $\rho(G_{6,3})$ .** We have shown in Section 5 that  $\partial_\infty D \cap \Omega$  is a solid torus  $T$ , and we have identified a simple closed curve in the boundary of  $T$  which bounds a disk  $\mathcal{E}$  in  $T$ .

**Proposition 6.1.** *The gray black curve and the red curve in  $\partial T$  in Figure 13 are isotopic in the torus  $\partial T$ .*

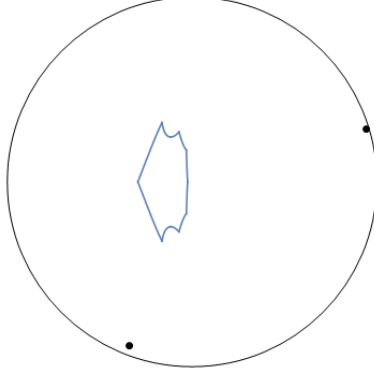


FIGURE 12. The projections of critical points and the disk  $\mathcal{E}$  onto the  $(t_2, t_3)$ -coordinates plane.

*Proof.* This is trivial when we glue the sides in Figure 13 to get a torus.  $\square$

So now the red curve in Figure 13 also bounds a disk in  $T$ . Now we cut  $T$  along this disk, we get a 3-ball  $B$ . Then the 3-orbifold  $\mathcal{O}$  at infinity of  $\rho(G_{6,3})$  is just the quotient space of  $B$  with side pairings as in Figure 13. We now show this with more details.

Each hexagon labeled by  $i$  (resp.  $\bar{i}$ ) for  $0 \leq i \leq 5$  in Figure 13 is part of the intersection of the bisector  $\mathcal{B}_i$  (resp.  $\mathcal{B}_{\bar{i}}$ ) and  $\mathbb{S}^3$ . Each bigon labeled by  $i$  (resp.  $\bar{i}$ ) for  $6 \leq i \leq 11$  in Figure 13 is part of the intersection of the bisector  $\mathcal{B}_i$  (resp.  $\mathcal{B}_{\bar{i}}$ ) and  $\mathbb{S}^3$ .

Figure 13 is a labeled disk. Here we denote the union of three green arcs (labeled by  $e_{13}$ ,  $e_{13}$  and  $e_{14}$ ) in the hexagons and bigon labeled by  $0$ ,  $\bar{0}$  and  $6$  by  $\beta_1$ , and we denote the union of three green arcs (labeled by  $e_{13}$ ,  $e_{13}$  and  $e_{14}$ ) in the hexagons labeled by  $1$  and  $\bar{1}$  by  $\beta_2$ . Then, by gluing  $\beta_1$  and  $\beta_2$  together, we get an annulus in the boundary of the 3-ball  $B$ , such that the two thick red curves bound disjoint disks in the boundary of the 3-ball  $B$ . The upper thick red curve in Figure 13 is denoted as  $A$ , and the lower thick red curve is denoted as  $A^{-1}$ . By abusing notation, we still use  $A$  to denote the identity map gluing the red curve  $A$  to the red curve  $A^{-1}$ , and  $A^{-1}$  to denote the inverse of  $A$ . Then we glue the disks enclosed by  $A$  and  $A^{-1}$  getting the solid torus  $T$ . Moreover, if we glue together the green paths, and then the red paths in Figure 13 (there is a twist when we glue the red circles, see the red edges labeled by  $e_{13}$ ), we get a torus, which is the boundary of the solid torus  $T$ .

For simplicity of notation, we write

$$g_i = \gamma_i \text{ and } g_{i+6} = \gamma_i \gamma_{i+1}^{-1},$$

where  $i = 0, 1, 2, 3, 4, 5$ .

Each  $g_i^{-1}$  maps the hexagon (or bigon) labeled by  $i$  to the hexagon (or bigon) labeled by  $\bar{i}$ , and  $A^{-1}$  maps the disk enclosed by  $A$  to the disk enclosed by  $A^{-1}$ . We now consider the actions of  $\{g_i\}_{0 \leq i \leq 11}$  on the edges in Figure 13:

- For  $i = 1$  (resp.  $i = 2$ ,  $i = 3$ ,  $i = 4$ ,  $i = 5$ ,  $i = 6$ ), the edge  $e_i$  lies on the  $\mathbb{C}$ -circle fixed by  $g_0$  (resp.  $g_5$ ,  $g_4$ ,  $g_3$ ,  $g_2$ ,  $g_1$ ), so the element  $g_0$  (resp.  $g_5$ ,  $g_4$ ,  $g_3$ ,  $g_2$ ,  $g_1$ ) fixes the edge  $e_1$  (resp.  $e_2$ ,  $e_3$ ,  $e_4$ ,  $e_5$ ,  $e_6$ );

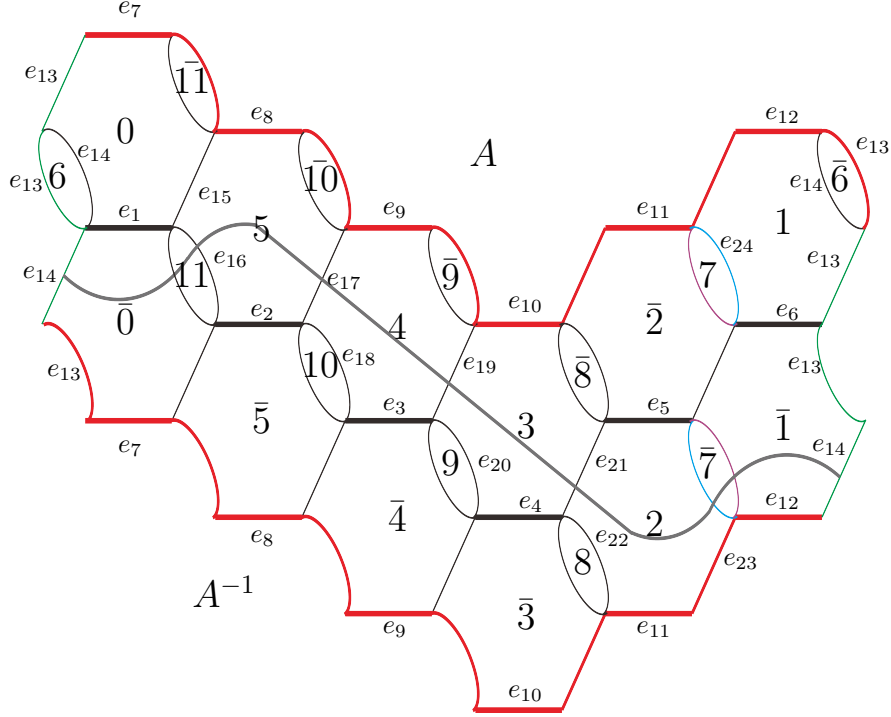


FIGURE 13. The gluing pattern for the 3-orbifold  $\mathcal{O}$ . The edges  $e_i$  and  $e_{i+6}$  for  $i = 1, 2, 3, 4, 5$  and  $6$  are on the  $\mathbb{C}$ -circles fixed by the isometries  $g_0, g_5, g_4, g_3, g_2$  and  $g_1$  respectively.

- The  $g_0^{-1}$ -image of the arc labeled by  $e_{14}$  in the boundary of the hexagon labeled by  $0$  is the green arc labeled by  $e_{14}$  in the boundary of the hexagon labeled by  $\bar{0}$ ;
- The  $g_0^{-1}$ -image of the green arc labeled by  $e_{13}$  in the boundary of the hexagon labeled by  $0$  is the red arc labeled by  $e_{13}$  in the boundary of the hexagon labeled by  $\bar{0}$ ;
- From the above two actions, we can easily get the full action of  $g_0^{-1}$  on the boundary arcs of the hexagon labeled by  $0$ ;
- Similarly, we have the action of  $g_i$  for  $i = 1, 2, 3, 4, 5$  on these hexagons;
- By taking sample points, we have the  $g_7^{-1}$ -image of the blue arc in the boundary of the bigon labeled by  $7$  (the intersection edge between the bigon labeled by  $7$  and hexagon labeled by  $1$ ) is the blue arc in the boundary of the bigon labeled by  $\bar{7}$  (the intersection edge between the bigon labeled by  $\bar{7}$  and hexagon labeled by  $2$ ); The  $g_7^{-1}$ -image of the purple arc in the boundary of the bigon labeled by  $7$  (the intersection edge between the bigon labeled by  $7$  and hexagon labeled by  $\bar{2}$ ) is the purple arc in the boundary of the bigon labeled by  $\bar{7}$  (the intersection edge between the bigon labeled by  $\bar{7}$  and hexagon labeled by  $\bar{1}$ );
- Similarly, we have the action of  $g_i$  for  $i = 6, 8, 9, 10, 11$  on these bigons.

From the side-pairings above, we get the 3-orbifold  $\mathcal{O}$  at infinity of  $\rho(G_{6,3})$ .

**6.2. A presentation of  $\pi_1(\mathcal{O})$ .** From the side-parings in Subsection 6.1, we will get a presentation of the fundamental group of the 3-orbifold  $\mathcal{O}$  in this subsection.

In Figure 13, we label the edge equivalent classes under the gluing pattern. But for the transparency of the figure, for some edge classes, we only label one of its representatives. Then we get a presentation of  $\pi_1(\mathcal{O})$  on thirteen generators

$$g_0, g_1, g_2, \dots, g_{11}, A$$

and twenty-four relations:

- the edge  $e_1$  (resp.  $e_2, e_3, e_4, e_5, e_6$ ) gives the relation  $(g_0^{-1})^3 = id$  (resp.  $(g_5^{-1})^3 = id, (g_4^{-1})^3 = id, (g_3^{-1})^3 = id, (g_2^{-1})^3 = id, (g_1^{-1})^3 = id$ );
- the edge  $e_7$  (resp.  $e_8, e_9, e_{10}, e_{12}$ ) gives the relation  $(Ag_0^{-1})^3 = id$  (resp.  $(Ag_5^{-1})^3 = id, (Ag_4^{-1})^3 = id, (Ag_3^{-1})^3 = id, (Ag_1^{-1})^3 = id$ ); and the edge  $e_{11}$  gives the relation  $(Ag_2)^3 = id$ ;
- there are twelve more relations given in Table 5.

TABLE 5. Some cycle relations of the 3-orbifold  $\mathcal{O}$ .

Ridge	Cycle relation
$e_{13}$	$g_1 g_6 A g_0^{-1}$
$e_{14}$	$g_0 g_1^{-1} g_6^{-1}$
$e_{15}$	$g_0 g_{11} A g_5^{-1}$
$e_{16}$	$g_5 g_0^{-1} g_{11}^{-1}$
$e_{17}$	$g_5 g_{10} A g_4^{-1}$
$e_{18}$	$g_4 g_5^{-1} g_{10}^{-1}$
$e_{19}$	$g_4 g_9 A g_3^{-1}$
$e_{20}$	$g_3 g_4^{-1} g_9^{-1}$
$e_{21}$	$g_3 g_8 g_2^{-1}$
$e_{22}$	$g_8 g_3 A^{-1} g_2^{-1}$
$e_{23}$	$g_2 g_7 g_1^{-1} A$
$e_{24}$	$g_7 g_2 g_1^{-1}$

Then we can cancel the generators  $g_6, g_7, \dots, g_{11}$  to give a presentation of  $\pi_1(\mathcal{O})$ :

$$\pi_1(\mathcal{O}) = \left\langle g_0, \dots, g_5, A \left| \begin{array}{l} g_i^3 = id, \quad (Ag_0^{-1})^3 = (Ag_1^{-1})^3 = (Ag_3^{-1})^3 = id, \\ (Ag_4^{-1})^3 = (Ag_5^{-1})^3 = (Ag_2)^3 = id, \\ Ag_0^{-1} g_1 g_0 g_1^{-1} = Ag_5^{-1} g_0 g_5 g_0^{-1} = Ag_4^{-1} g_5 g_4 g_5^{-1} = id, \\ Ag_3^{-1} g_4 g_3 g_4^{-1} = Ag_3^{-1} g_2^{-1} g_3 g_2 = Ag_2 g_1 g_2^{-1} g_1^{-1} = id \end{array} \right. \right\rangle.$$

We should remark here the presentation of  $\pi_1(\mathcal{O})$  is not symmetric with the generators above, and moreover if we add the relation  $A = id$  to  $\pi_1(\mathcal{O})$ , then we get the original group  $G_{6,3}$ .

Using the Magma Calculator available at [17], we can simplify the presentation to get

$$(6.1) \quad \pi_1(\mathcal{O}) = \left\langle s_1, \dots, s_6 \left| \begin{array}{l} s_i^3 = id, \quad s_2 s_1^{-1} s_2^{-1} s_1 s_6^{-1} s_1 s_6 s_1^{-1} = id, \\ s^{-1} s_2 s_1 s_3 s_2^{-1} s_3^{-1} = id, \quad s_5 s_4 s_5^{-1} s_3^{-1} s_4^{-1} s_3 = id, \\ s_6 s_5^{-1} s_6^{-1} s_5 s_1^{-1} s_2 s_1 s_2^{-1} = id, \quad s_2 s_1^{-1} s_2^{-1} s_1 s_4^{-1} s_5 s_4 s_5^{-1} = id \end{array} \right. \right\rangle.$$



Changing  $u_3 = s_2 s_3 s_2^{-1}$ ,  $s_3 = s_2^{-1} u_3 s_2$ ,  $u_i = s_i$  for  $i = 1, 2, 4, 5, 6$ , we can rewrite the presentation as

$$(6.2) \quad \pi_1(\mathcal{O}) = \left\langle u_1, u_2, u_3, u_4, u_5, u_6 \left| \begin{array}{l} u_i^3 = id, \quad u_3 u_2^{-1} u_3^{-1} u_2 = u_2 u_1^{-1} u_2^{-1} u_1 = id, \\ u_1 u_6^{-1} u_1^{-1} u_6 = u_6 u_5^{-1} u_6^{-1} u_5 = id, \\ u_5 u_4^{-1} u_5^{-1} u_4 = u_5 u_4 u_5^{-1} u_2^{-1} u_3^{-1} u_2 u_4^{-1} u_2^{-1} u_3 u_2 = id \end{array} \right. \right\rangle.$$

**6.3. A chain link orbifold.** Consider the link in Figure 14, it is called the chain link  $C(6, -2)$  in [19] (in fact, our link here is the mirror image of the link  $C(6, -2)$  in [19], but this does not matter, since they have homeomorphic complements.)

Then from the standard Wirtinger presentation of the fundamental group of a link in the 3-sphere [20], we see that  $\pi_1(\mathbb{S}^3 - C(6, -2))$  is a group on fourteen generators

$$y_0, \dots, y_6, z_0, \dots, z_6$$

and fourteen relations in Table 6.

TABLE 6. Relations of  $\pi_1(\mathbb{S}^3 - C(6, -2))$ .

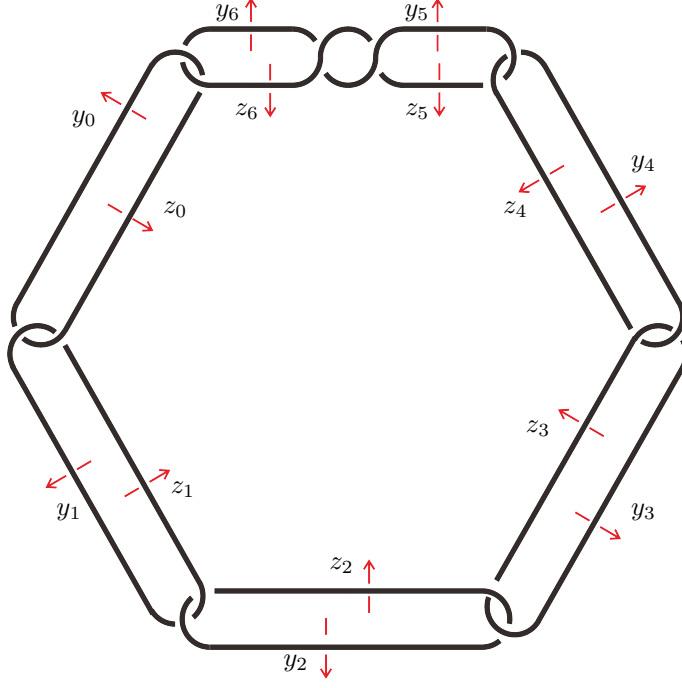
crossing	relation
1	$z_6 y_0 y_6^{-1} y_0^{-1}$
2	$z_6 z_0 z_6^{-1} y_0^{-1}$
3	$z_0 y_1 y_0^{-1} y_1^{-1}$
4	$z_0 z_1 z_0^{-1} y_1^{-1}$
5	$z_1 y_2 y_1^{-1} y_2^{-1}$
6	$z_1 z_2 z_1^{-1} y_2^{-1}$
7	$z_2 y_3 y_2^{-1} y_3^{-1}$
8	$z_2 z_3 z_2^{-1} y_3^{-1}$
9	$z_3 y_4 y_3^{-1} y_4^{-1}$
10	$z_3 z_4 z_3^{-1} y_4^{-1}$
11	$z_4 y_5 y_4^{-1} y_5^{-1}$
12	$z_4 z_5 z_4^{-1} y_5^{-1}$
13	$z_5 z_6 z_5^{-1} y_6^{-1}$
14	$y_5 z_6 y_5^{-1} z_5^{-1}$

Here the relations  $z_5 z_6 z_5^{-1} y_6^{-1}$  and  $y_5 z_6 y_5^{-1} z_5^{-1}$  correspond to the two crossings in the twist region of Figure 14, so they have different forms from those of the others.

We consider the 3-orbifold  $\mathcal{L}$  with underlying space the 3-sphere and whose singular locus is the  $\mathbb{Z}_3$ -coned chain-link  $C(6, -2)$ . Then its fundamental group is just add the relations  $y_i^3 = z_i^3 = id$  for  $i = 0, 1, 2, 3, 4, 5, 6$  to the presentation  $\pi_1(\mathbb{S}^3 - C(6, -2))$  above.

Using Magma [17], we can simplify the presentation of  $\pi_1(\mathcal{L})$  to get

$$\pi_1(\mathcal{L}) = \left\langle t_1, \dots, t_6 \left| \begin{array}{l} t_i^3 = id, \quad t_5^{-1} t_6 t_5 t_6^{-1} t_4 t_3^{-1} t_4^{-1} t_3 = t_5^{-1} t_6 t_5 t_6^{-1} t_2 t_1^{-1} t_2^{-1} t_1 = id, \\ t_2^{-1} t_3 t_2 t_3^{-1} t_6 t_5^{-1} t_6^{-1} t_5 = t_5^{-1} t_6 t_5 t_6^{-1} t_5 t_4^{-1} t_5^{-1} t_4 = id, \\ t_1^{-1} t_2 t_1 t_2^{-1} t_3 t_2^{-1} t_3^{-1} t_2 = t_2 t_1 t_2^{-1} t_5^{-1} t_6^{-1} t_5 t_1^{-1} t_5^{-1} t_6 t_5 = id \end{array} \right. \right\rangle.$$

FIGURE 14. The Chain link  $C(6, -2)$ .

We can rewrite it as

$$(6.3) \quad \pi_1(\mathcal{L}) = \left\langle t_1, \dots, t_6 \left| \begin{array}{l} t_i^3 = id, \quad t_6 t_5^{-1} t_6^{-1} t_5 = t_5 t_4^{-1} t_5^{-1} t_4 = id, \\ t_4 t_3^{-1} t_4^{-1} t_3 = t_3 t_2^{-1} t_3^{-1} t_2 = id, \\ t_2 t_1^{-1} t_2^{-1} t_1 = t_2 t_1 t_2^{-1} t_5^{-1} t_6^{-1} t_5 t_1^{-1} t_5^{-1} t_6 t_5 = id \end{array} \right. \right\rangle.$$

Now the map  $f : \pi_1(\mathcal{L}) \rightarrow \pi_1(\mathcal{O})$ ,

$$(6.4) \quad \begin{aligned} t_1 &\rightarrow u_4, \\ t_2 &\rightarrow u_5, \\ t_3 &\rightarrow u_6, \\ t_4 &\rightarrow u_1, \\ t_5 &\rightarrow u_2, \\ t_6 &\rightarrow u_3, \end{aligned}$$

is an isomorphism between  $\pi_1(\mathcal{L})$  in the presentation (6.3) and  $\pi_1(\mathcal{O})$  in the presentation (6.2).

Now we take a torsion free finite index subgroup of  $\pi_1(\mathcal{L}) = \pi_1(\mathcal{O})$ , which corresponds to finite covers  $\tilde{\mathcal{L}} \rightarrow \mathcal{L}$  and  $\tilde{\mathcal{O}} \rightarrow \mathcal{O}$ . We will show in Subsection 6.4 that  $\mathcal{L}$  is a closed hyperbolic 3-orbifold. So  $\tilde{\mathcal{L}}$  is a closed hyperbolic 3-manifold. Then, by the prime decompositions of 3-manifolds [13],  $\tilde{\mathcal{O}}$  is the connected sum of  $\tilde{\mathcal{L}}$  with  $\mathcal{N}$ , where  $\mathcal{N}$  is a closed 3-manifold with trivial fundamental group. By the solution of the Poincaré Conjecture, then  $\mathcal{N}$  is the 3-sphere, so  $\tilde{\mathcal{L}}$  is homeomorphic to  $\tilde{\mathcal{O}}$ . This in turn implies  $\mathcal{L}$  is homeomorphic to  $\mathcal{O}$ . This finishes the proof of the first part of Theorem 1.2.

**6.4. Hyperbolicity of the 3-orbifold  $\mathcal{O}$ .** We show the orbifold  $\mathcal{O}$  is hyperbolic by the arguments from Cooper-Hodgson-Kerckhoff [3] and Dunbar [8]. From Theorem 1.25 of [3], we see  $\mathcal{O}$  is a geometric 3-orbifold. That is, the 3-orbifold with underlying space  $\mathbb{S}^3$  and  $\mathbb{Z}_3$ -coned singular set on  $C(6, -2)$  is a geometric 3-orbifold. In page 81 of [8], there is classification of non-hyperbolic 3-orbifold with underlying space  $\mathbb{S}^3$ . There is no orbifold with singular set a  $\mathbb{Z}_3$ -coned six components link in the list.  $\mathcal{O}$  is hyperbolic, since it is not one of the exceptions. We thank one of the referees for pointing this out to us.

This completes the proof of Theorem 1.2.

#### REFERENCES

- [1] M. Acosta. Spherical CR uniformization of Dehn surgeries of the Whitehead link complement. *Geom. Topol.* 23(2019), 2593–2664.
- [2] M. Bourdon. Immeubles hyperboliques, dimension conforme et rigidité de Mostow. (French) [Hyperbolic buildings, conformal dimension and Mostow rigidity] *Geom. Funct. Anal.* 7 (1997), no. 2, 245–268.
- [3] D. Cooper, C. Hodgson, S. Kerckhoff. Three Dimensional Orbifolds and Cone Manifolds. *Proc. Japan Math. Soc.* 5 (2000).
- [4] M. Deraux. On spherical CR uniformization of 3-manifolds. *Exp. Math.* 24(2015), 355–370.
- [5] M. Deraux. Deforming the  $\mathbb{R}$ -Fuchsian  $(4, 4, 4)$ -triangle group into a lattice. *Topology* 45(2006), 989–1020.
- [6] M. Deraux and E. Falbel. Complex hyperbolic geometry of the figure eight knot. *Geom. Topol.* 19(2015), 237–293.
- [7] M. Deraux, J. R. Parker and J. Paupert. New non-arithmetic complex hyperbolic lattices. *Invent. Math.* 203 (2016), 681–771.
- [8] W. D. Dunbar. Geometric orbifolds. *Rev. Mat. Univ. Complut. Madrid* 1(1988), no. 1-3, 67–99.
- [9] W. M. Goldman. *Complex Hyperbolic Geometry*. Oxford Mathematical Monographs. Oxford University Press, 1999.
- [10] W. M. Goldman. and J. R. Parker. Complex hyperbolic ideal triangle groups. *J. Reine Angew. Math.* 425(1992), 71–86.
- [11] J. Granier. Groupes discrets en géométrie hyperbolique—Aspects effectifs. PhD thesis, Université de Fribourg, 2015.
- [12] M. Gromov. *Hyperbolic groups*. Essays in group theory, 75–263, Math. Sci. Res. Inst. Publ., 8, Springer, New York, 1987.
- [13] J. Hempel. *3-manifolds*. Reprint of the 1976 original. AMS Chelsea Publishing, Providence, RI, 2004.
- [14] Y. Jiang, J. Wang and B. Xie. A uniformizable spherical CR structure on a two-cusped hyperbolic 3-manifold. *Algebr. Geom. Topol.* 23(2023), 4143–4184.
- [15] M. Kapovich. A survey of complex hyperbolic Kleinian groups. In: *In The Tradition of Thurston II. Geometry and Groups*, pp. 7–51. Springer, Cham (2022).
- [16] J. Ma and B. Xie. Three-manifolds at infinity of complex hyperbolic orbifolds. arXiv:2205.11167.
- [17] Magma Computational Algebra System, <http://magma.maths.usyd.edu.au/magma/>
- [18] G. D. Mostow. On a remarkable class of polyhedra in complex hyperbolic space. *Pacific J. Math.* 86 (1980), 171–276.
- [19] W. D. Neumann and A. W. Reid. Arithmetic of hyperbolic manifolds. *Topology '90* (Columbus, OH, 1990), 273–310, Ohio State Univ. Math. Res. Inst. Publ., 1, de Gruyter, Berlin, 1992.
- [20] D. Rolfsen. *Knots and links*. Corrected reprint of the 1976 original. Mathematics Lecture Series, 7. Publish or Perish, Inc., Houston, TX, 1990.
- [21] J. R. Parker, J. Wang and B. Xie. Complex hyperbolic  $(3, 3, n)$  triangle groups. *Pacific J. Math.* 280(2016), 433–453.
- [22] J. R. Parker and P. Will. A complex hyperbolic Riley slice. *Geom. Topol.* 21 (2017), 3391–3451.

- [23] R. E. Schwartz. Ideal triangle groups, dented tori, and numerical analysis. *Ann. of Math.* (2)153 (2001), no. 3, 533–598.
- [24] R. E. Schwartz. Degenerating the complex hyperbolic ideal triangle groups. *Acta Math.* 186(2001), no. 1, 105–154.
- [25] R. E. Schwartz. Complex hyperbolic triangle groups. Proceedings of the International Congress of Mathematicians. (2002) Volume 1: Invited Lectures, 339–350.
- [26] R. E. Schwartz. Real hyperbolic on the outside, complex hyperbolic on the inside. *Invent. Math.* 151(2003), no. 2, 221–295.
- [27] R. E. Schwartz. A better proof of the Goldman-Parker conjecture. *Geom. Topol.* 9(2005), 1539–1601.

SCHOOL OF MATHEMATICAL SCIENCES, FUDAN UNIVERSITY, SHANGHAI, 200433, P. R. CHINA  
*Email address:* `majiming@fudan.edu.cn`

SCHOOL OF MATHEMATICS, HUNAN UNIVERSITY, CHANGSHA, 410082, CHINA  
*Email address:* `xiexbh@hnu.edu.cn`